AD-A182 960 RESEARCH AND CRYSTAL GROWTH ON HIGH DIELECTRIC CONSTANT 1/1
MATERIALS FOR MIL.. (U) STANFORD UNIV CA CENTER FOR
MATERIALS RESEARCH R S FEIGELSON 05 JUN 87 CMR-87-2
UNCLASSIFIED N00014-82-K-0266 F/G 20/2 NL

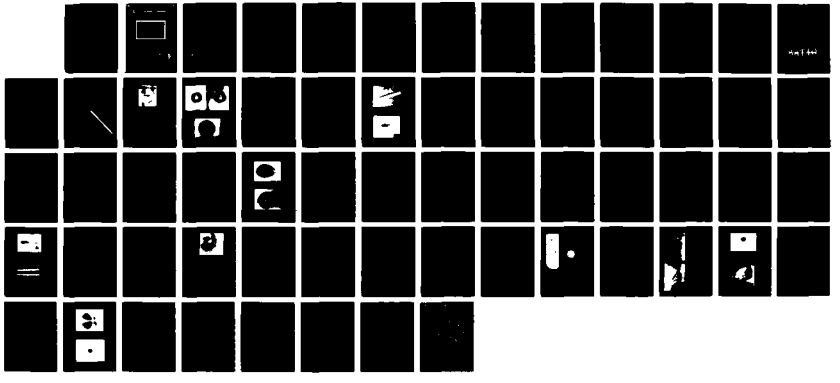

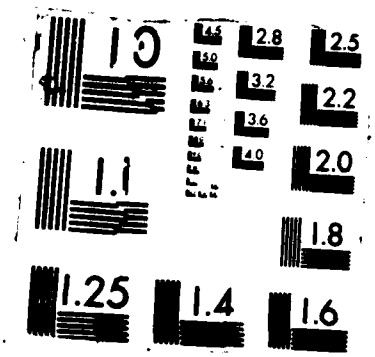
1.0
1.1
1.25
1.4
1.6
1.8
2.0
2.2
2.5
2.8
3.2
3.6
4.0
4.5
5.0

(12)

Final Technical Report

on

Research and Crystal Growth on

High Dielectric Constant Materials

for Millimeter Wave Applications

for the period

3/01/82 through 9/30/86

Contract Number N00014-82-K-0266

CMR-87-2

CENTER FOR MATERIALS RESEARCH

STANFORD UNIVERSITY • STANFORD, CALIFORNIA

12

The Board of Trustees of the
Leland Stanford Junior University
Center for Materials Research
Stanford, CA 94305
Santa Clara, 12th Congressional District

Final Technical Report

on

Research and Crystal Growth on High Dielectric Constant Materials for Millimeter Wave Applications

for the period

3/01/82 through 9/30/86

Contract Number N00014-82-K-0266

CMR-87-2

Submitted to
The Office of Naval Research

Principal Investigator

Robert S. Feigelson
Professor (Research)
Center for Materials Research
Crystal Science and Engineering

June 5, 1987

TABLE OF CONTENTS

RESEARCH AND CRYSTAL GROWTH ON HIGH DIELECTRIC CONSTANT MATERIALS FOR MILLIMETER WAVE APPLICATIONS

Abstract

The primary objective of this program was the growth of high quality single crystals for evaluation as potential candidates for electro-optic phase shifters in millimeter-wave applications. The research program was initially conceived as two parallel efforts. The first involved the application of new crystal growth techniques to the growth of strontium-barium titanate solid solutions. These materials are promising for the above applications but have been difficult to grow in the form of high quality single crystals. The second part of this program involved a study of some newly discovered ferroelectric materials; the ternary heavy metal fluorides and the niobates and tantalates of scandium. During the first year, it was decided that this latter effort should become the main focus of the program.

Several types of crystal growth techniques were employed during this program including the Bridgman, top-seeded flux, and laser-heated pedestal growth methods. During the course of this investigation, crystals of $ScTaO_4$, $ScNbO_4$, $SrAlF_5$, $Pb_3Al_2F_{12}$ ($PbAlF_5$), $BaTiO_3$, and $Sr_xBa_{1-x}TiO_3$ solid solutions were grown. The $ScTaO_4$ crystals grown in this program were of a previously undiscovered high temperature tetragonal phase. High quality $BaTiO_3$ crystals in the metastable, high temperature hexagonal phase were also produced. Large crystals of $SrAlF_5$ were grown by the Bridgman method, but the material lacks a high dielectric constant at mm wave frequencies and studies on this material were not pursued. More promising materials in the PbF_2-AlF_3 and PbF_2-GaF_3 systems became the focus of our attention during the later part of this program. A large crystal of $Pb_3Al_2F_{12}$ was grown and some of its properties measured. Some crystals of this material contained optical inhomogeneities, and the resulting microstructure may have been due to the presence of secondary phases or oxygen contamination. Thermodynamic studies, synthesis and purification techniques, and crystal growth of compositions in the PbF_2-AlF_3 system are described.

RESEARCH AND CRYSTAL GROWTH ON HIGH DIELECTRIC CONSTANT MATERIALS FOR MILLIMETER WAVE APPLICATIONS

I. GENERAL INTRODUCTION

This research program, initially for three-years beginning in March 1982, was continued through to September 1986 with the use of no-cost extensions and a small amount of additional financial support for one graduate student.

A. Objectives

The primary objective of this program was the growth of high quality single crystals for evaluation as potential candidates for mm wave applications. This research program was initially conceived as two parallel efforts. The first, which was discontinued after the first year, involved the application of new crystal growth techniques to the growth of strontium-barium titanate solid solutions, traditionally difficult to grow as high quality single crystals. The second effort involved a study of two newly discovered classes of materials; the ternary heavy metal fluorides and the niobates and tantalates of scandium.

B. Background

In recent years there has been increased interest in electrically controlled phase shifters in the near-millimeter spectral region for radar and communications applications. Lower frequency phase shifters such as the ferrites or loaded waveguide structures either become lossy or have power handling problems at increasing frequencies. Phase shifters using the electro-optic effect in bulk crystals are commonly used in visible wavelengths and have speeds limited only by circuit conditions. They have a number of features which make them attractive in the near-millimeter spectral region as well.

The phase shift for a transverse electro-optic modulator is given [1] by

$$\Gamma = \frac{\pi L}{\lambda} \frac{V}{D} \quad n^3 r$$

where L = crystal length, V = applied voltage, D = electrode spacing, n = microwave refraction index, and r = the electro-optic coefficient. A figure of merit can be expressed as

$$R = n^3 r$$

For optimum performance, one desires a crystalline material with high values of the microwave index of refraction and electro-optic coefficients. It has also been shown [2,3] that crystals with high microwave electro-optic coefficients are those with the highest values of linear dielectric susceptibility, which in low loss materials means those materials with large values of the low frequency dielectric constant. In preliminary calculations, Klein [1] has shown that the strong ferroelectrics such as $BaTiO_3$, $LiNbO_3$, etc., appear to be the most promising materials. Solid solutions of strontium-barium titanate are particularly interesting because, depending on composition, the Curie temperature can be varied from below room temperature to 130°C; and it is at temperatures near the Curie point where one obtains very large values for the dielectric constants.

While this program was on-going, the Chinese [4] reported on a new high dielectric constant material, $ScTaO_4$. Using our unique laser-heated pedestal growth technology, which is based on the float-zone method, we grew single crystals of $ScTaO_4$ from a pure melt (for the first time) and discovered a new high temperature phase. We also grew, by this method, crystals of $ScNbO_4$ (never grown before), the high temperature hexagonal phase of $BaTiO_3$ and solid solutions in the $Sr_xBa_{1-x}TiO_3$ system.

Although oxides comprise by far the largest fraction of known ferroelectrics, several new classes of materials have recently appeared which may have potential in dielectric applications and which present challenging materials problems. These include the ferroelectric fluorides of the type ABF_5 and $A_3B_2F_{12}$ (A = Sr, Ba, Pb; B = Al, Ga, In) which were found to be particularly interesting because the exact nature of their ferroelectric behavior is not well understood, and also because they may have very useful properties for a

variety of device applications. $SrAlF_5$ and $SrGaF_5$, for example, are currently important candidate materials for tunable high power solid-state laser applications, and some of the family members have potentially useful properties for mm wave applications.

Interest in fluoride ferroelectrics developed when the ferroelectric behavior of certain compounds in the $SrAlF_5$ family was reported [5,6]. While very few fluorides have definitely been established to be ferroelectric, such as $LiN_2H_5BeF_4$ [7], the evidence supporting the claim that some members of the $SrAlF_5$ family are polar and undergo a phase transition is fairly strong. Measurements on these materials, however, were made on polycrystalline samples and definite proof of this ferroelectric behavior is still lacking. In our program we studied two of these ferroelectric fluorides; $SrAlF_5$, for which a successful growth technique was developed and some preliminary property measurements made on the single crystal samples produced, and compounds in the PbF_2-AlF_3 system, which may have even more interesting dielectric properties. In this latter study we encountered a controversy surrounding the existence of two of the reported compounds, $PbAlF_5$ and $Pb_3Al_2F_{12}$. Part of this controversy concerned the question of oxygen and H_2O contamination. High quality, pure crystals would help resolve this question.

We thought it appropriate after about a year into this program to redirect most of our research effort to an investigation on the growth of very pure, high quality single crystals of several of the tetragonal ternary fluoride compounds, in particular those in the PbF_2-AlF_3 and PbF_2-GaF_3 systems and attempt to firmly establish that these materials are truly ferroelectric. Single crystals will permit a careful comparison between experiment and theory and hopefully will help in the development of a real understanding of fluoride ferroelectrics. In addition to single crystal growth and property measurements, it was found necessary to devote considerable effort to the purification of the starting materials used for growth (removal of oxide impurites being especially important) handling procedures for these materials and producing accurate PbF_2-AlF_3 and PbF_2-GaF_3 phase diagrams.

Finally, we planned to make an assessment of the suitability of compounds in the $SrAlF_5$ family for device applications. Difficulties in

the growth and characterization phases, however, have delayed this part of the program.

II. OXIDE FERROELECTRICS

A. Barium Titanate-Strontium Titanate Solid Solutions

1. Introduction

$BaTiO_3$-$SrTiO_3$ solid solutions possess large values of dielectric permittivity and a Curie temperature which can be varied from below room temperature to 135°C [8]. High quality (homogeneous) crystals of these solid solutions are difficult to grow because of high temperatures involved, chemical reactivity, and segregation behavior. The $BaTiO_3$-$SrTiO_3$ phase diagram [9] is shown in fig. 1. While this system exhibits complete solid solubility, melts can be crystallized without segregation only at the minimum melting composition (1585°C). If a melt containing a greater concentration of $SrTiO_3$ is crystallized, for example at 20% $SrTiO_3$, the composition of the solid formed on cooling, as indicated by point A in fig. 1, will be richer in $SrTiO_3$ than the melt from which it grows (32% $SrTiO_3$ in this illustration). As a result, the melt becomes slightly depleted in $SrTiO_3$ and the next material to crystallize does so from a melt containing excess $BaTiO_3$. For this reason the crystal and melt both change composition as indicated by the arrows on the liquidus and solidus curves in fig. 1. This phenomenon gives rise to crystals with inhomogenous compositions.

Crystals of $BaTiO_3$, $SrTiO_3$, and their solid solutions are usually grown from solutions containing excess TiO_2. This lowers growth temperatures to convenient levels, and in the case of $BaTiO_3$ below the high temperature hexagonal-cubic phase transformation temperature. Solution growth processes lead to slow growth rates and difficulty in controlling nucleation. For $Ba_{1-x}Sr_xTiO_3$ traditional Czochralski and bulk float-zone techniques have been tried, but not with outstanding success [10]. Growth of $Ba_{1-x}Sr_xTiO_3$ crystals from TiO_2-rich solutions also produced graded compositions, and in addition, interface breakdown and second phase inclusions were common.

Melt stirring in solution growth improves interface stability by helping to bring nutrient to the growth interface. The accelerated crucible rotation

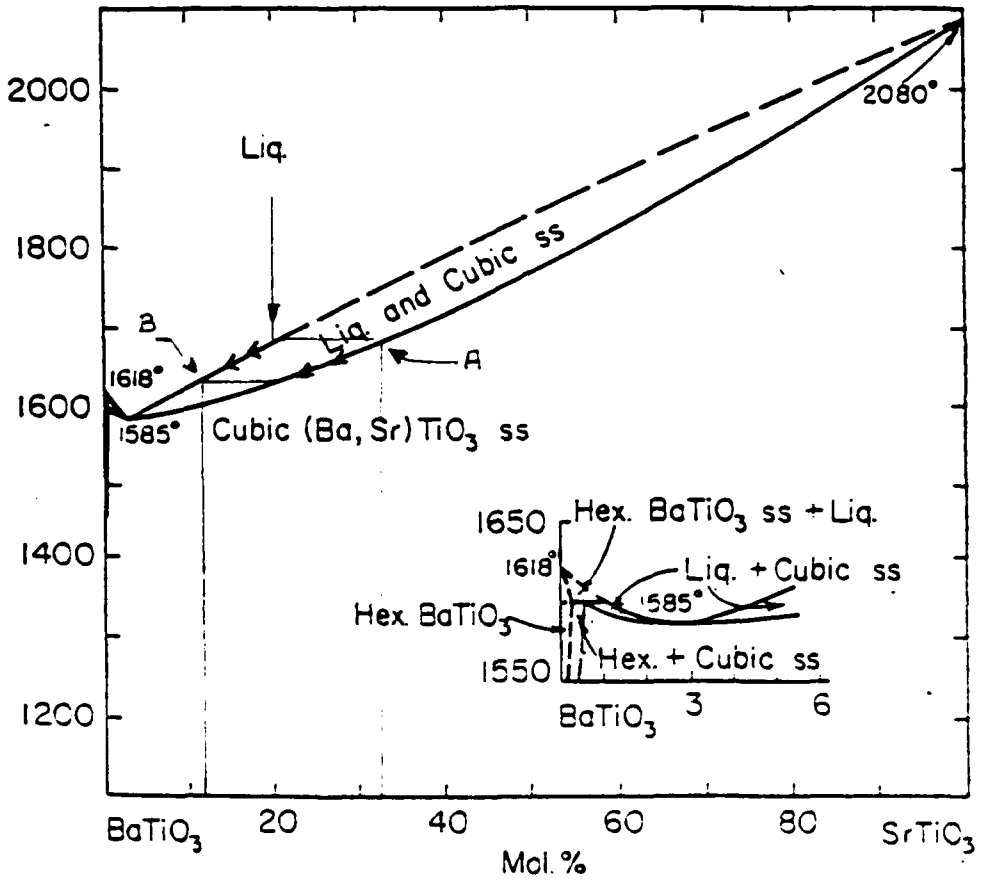

Fig. 1: $BaTiO_3$-$SrTiO_3$ phase diagram [9].

technique (ACRT) [11] and a new stirring method being studied in our laboratory known as coupled vibrational stirring [12] were developed for stirring melts during high temperature growth processes where other methods are unsuitable. It was the original intention of this part of the program to apply these techniques to the growth of homogeneous solid solutions of $Ba_{1-x}SrTiO_3$.

Two approaches were used to grow $BaTiO_3$ and $Ba_{1-x}Sr_xTiO_3$ solid solutions. One involved the growth of small diameter crystals using our unique laser-heated pedestal growth (LHPG) technology [13] (a variation of the float-zone process). This technique has been applied to a wide variety of materials and is ideal for growing solid solutions of uniform composition. In pedestal growth, a source rod of the composition desired (take for example the 20% $SrTiO_3$ composition as discussed earlier) is continuously added to the melt as growth proceeds. When the melt composition reaches point B (fig. 1), which will be about 12% $SrTiO_3$, the composition of the material crystallizing from this melt will be 20% $SrTiO_3$, the desired composition. Since we are now continuously adding material to the melt of the same composition that is being pulled from it, a steady-state condition is reached. Under these circumstances the melt composition remains at a constant value of 12% $SiTiO_3$. A number of congruently and incongruently melting oxides have already been grown in high-quality single-crystal form by the LHPG method including $LiNbO_3$ and Yttrium Iron Garnet (YIG) which is incongruently melting. Materials which are incongruently melting or which must be grown from solution for other reasons (phase transformations, high vapor pressure, etc.) are somewhat more difficult to grow due to mass transport and melt stability problems.

A second technique studied for the growth of the oxide ferroelectrics described above was the top-seeded version of the flux growth method. This method had been developed for the growth of cm-sized $BaTiO_3$ crystals using excess TiO_2 as the flux [14]. The top-seeded solution growth technique, like other solution growth methods, requires very slow growth rates. It was our idea to apply melt stirring techniques in order to increase growth rates and

also to improve the uniformity of the $Ba_{1-x}Sr_xTiO_3$ crystals grown by this method. While this was one of the original goals of the program, it became clear it was too ambitious an undertaking given the limited resources available, We therefore abandoned this effort early on in favor of the LHPG growth of the ferroelectric oxides discussed above and growth of the ferroelectric fluorides.

2. Single Crystal Growth by the LHPG Method

A schematic of the laser-heated pedestal growth method is illustrated in fig. 2. This new, unique crystal growth technology was found [13] to be a very powerful tool for preparing small diameter single crystals for physical property evaluation. Its desirable features for this application include: 1) ease of operation, 2) fast growth rates, 3) large quantities of material are not needed, and 4) no crucibles or furnaces are required.

Source rods of the materials to be grown were fabricated into bars 1-2 mm square from hot-pressed or cold-pressed and sintered polycrystalline ceramics made in our laboratory. The top of this source rod was melted with a 50 watt CO_2 laser and the crystal, usually with a diameter between 0.5 - 2 mm was pulled from this molten zone as shown in fig. 2b. Growth rates of 0.1 to 1 mm/min are typically used depending on whether a pure melt or solution was used. More detailed information in the LHPG method is given in [15].

The first LHPG growth experiments in this program were carried out with pure $BaTiO_3$. When grown by this method from pure stoichiometric melts, the small diameter $BaTiO_3$ crystals did not, as will larger crystals grown by other methods, undergo the destructive hexagonal to cubic phase transformation. Instead the high temperature hexagonal structure persisted to room temperature. One of these crystals is shown in fig. 3. The rapid growth rates and steep axial temperature gradients used in the LHPG growth of small diameter crystals are much higher than most bulk growth methods, and effectively leads to quenching in of the high temperature phase. The low temperature ferroelectric phase of $BaTiO_3$ was also grown using laser-heated pedestal growth together with a TiO_2-rich solution. This solution, as mentioned previously, lowers the solidification temperature to below the

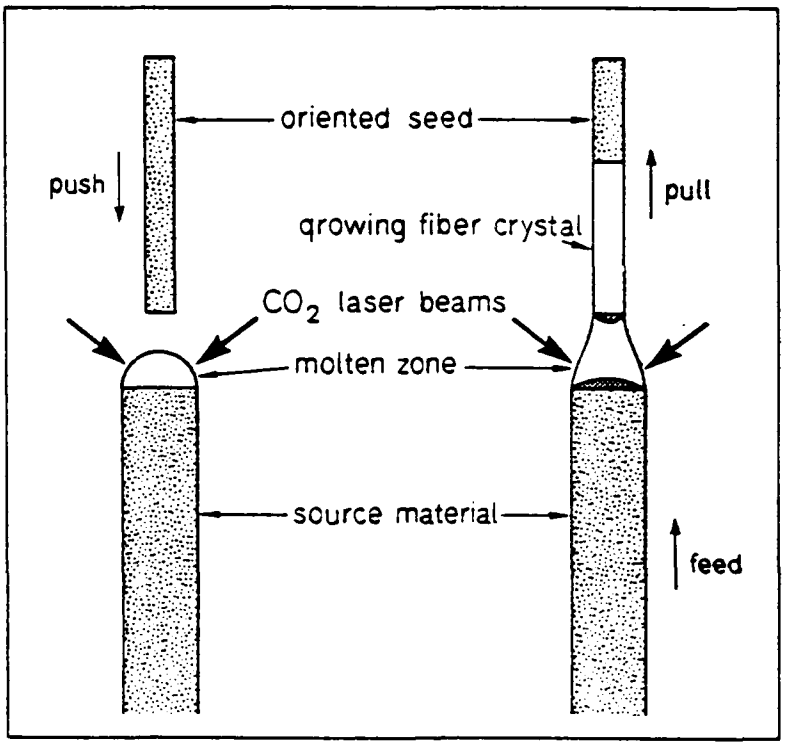

Fig. 2: Schematic illustration of the laser-heated pedestal growth method [13].

Fig. 3: Single crystal of hexagonal $BaTiO_3$ grown by the LHPG method from pure melt.

transformation temperature. One fiber grown by this technique is shown in fig. 4. Fiber crystals of $Sr_{.25}Ba_{.75}TiO_3$ and $Sr_{.5}Ba_{.5}TiO_3$ are shown in fig. 5. They were grown from nominally pure melts (i.e. no excess TiO_2). The $Sr_{.5}Ba_{.5}TiO_3$ fibers, while single crystals, contained light scattering centers, the cause of which was not investigated.

Due to the difficulty involved in making dielectric measurements on these small diameter samples, and also the shift in emphasis of the program, these fibers were not evaluated.

3. Top-Seeded Flux Growth

Attempts were made to grow $BaTiO_3$ crystals using the top-seeded growth method and a TiO_2-rich melt. A platinum crucible was located inside a well-insulated specially built SiC element furnace as shown in fig. 6. The rotating seed crystal was cooled by air blown down the rod holding it. The $BaO-TiO_2$ phase diagram [16] is shown in fig. 7. In order to obtain pure $BaTiO_3$ in the cubic phase, a solution containing about 65 mole % TiO_2 is needed. Crystallization from this melt composition starts at about 1500°C. As the solution is cooled the melt becomes richer in TiO_2 and the melt composition approaches the eutectic composition where two solid phases crystallize from the solution. If the growth rates are too fast,the composition at the interface can prematurely reach the eutectic composition and inclusions and other defects can form. After considerable modifications to the furnace, large grained polycrystalline boules of $BaTiO_3$ and $Sr_{0.12}Ba_{0.88}TiO_3$ (as shown in fig. 8) were obtained from this apparatus. Unfortunately, since the growth temperatures are around 1500°C, a large amount of insulation was required to keep the SiC elements from overheating. This led to very low radial thermal gradients and, thus, difficulty in controlling the crystal diameter and solid-liquid interface shape. The resulting crystals were not of high quality due to these poor growth conditions. Had this phase of the program continued, the furnace would have been rebuilt using $MoSi_2$ elements which can withstand higher temperatures than SiC, thus permitting steeper gradients.

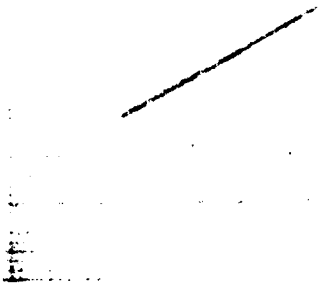

Fig. 4: Solution-grown single crystal of low temperature phase of $BaTiO_3$ using excess TiO_2 in molten zone (mm scale).

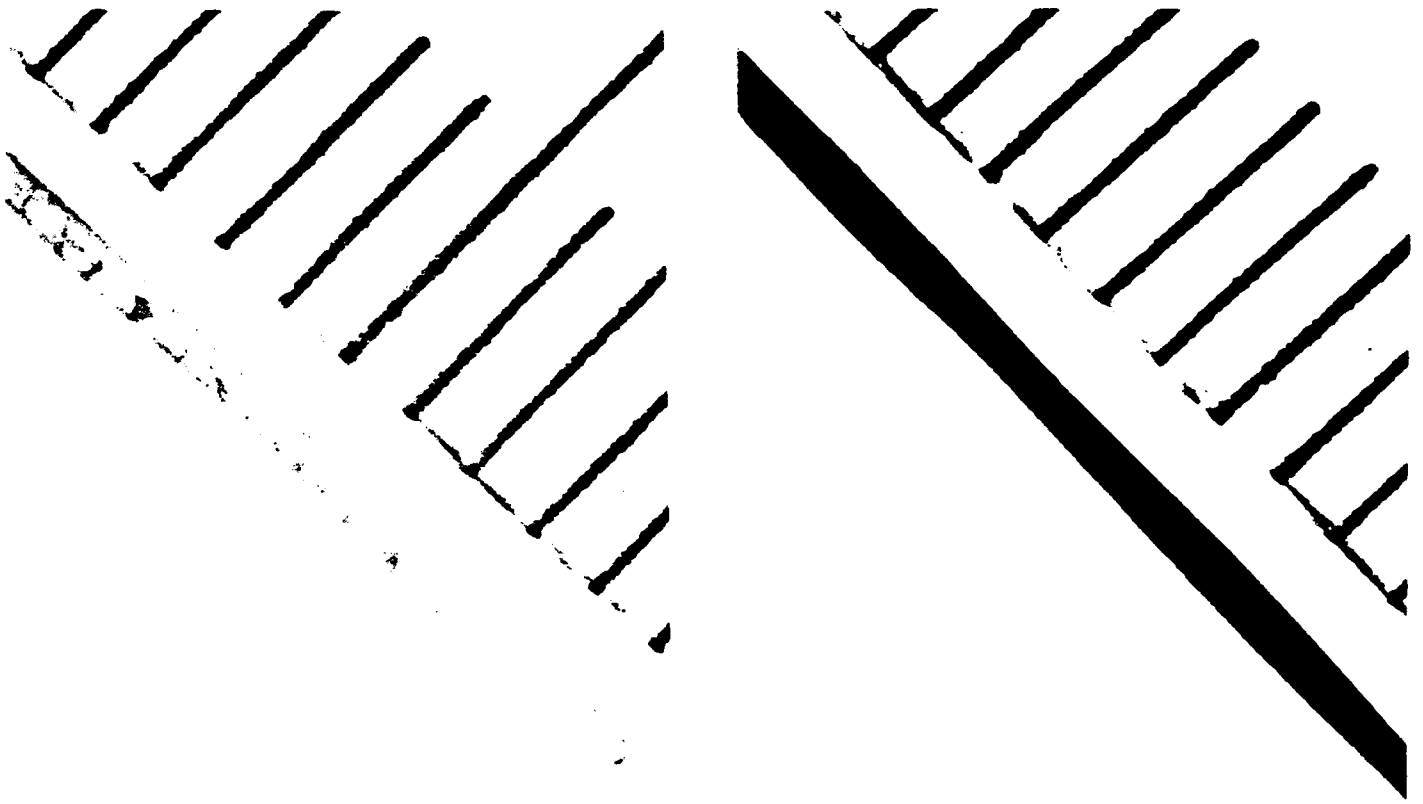

Fig. 5: Single crystals of $Sr_{.25}Ba_{.75}TiO_3$ (left) and $Sr_{.5}Ba_{.5}TiO_3$ (right) grown from pure melt.

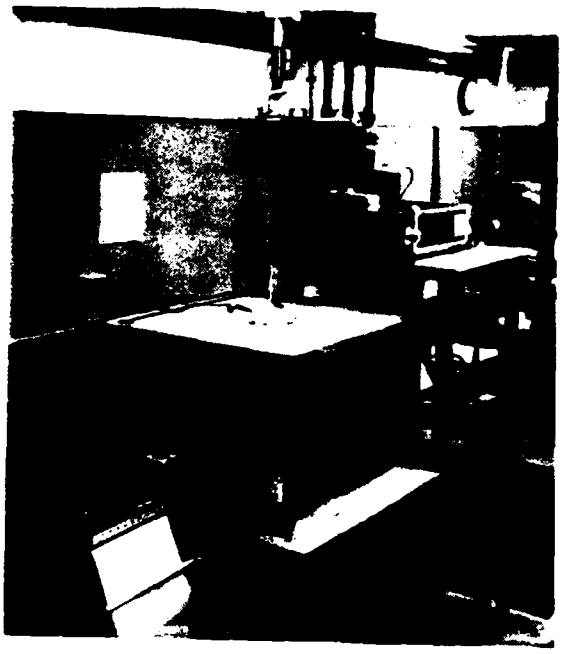

Fig. 6: SiC furnace built for top-seeded solution growth of $BaTiO_3$-$SrTiO_3$ solid solutions.

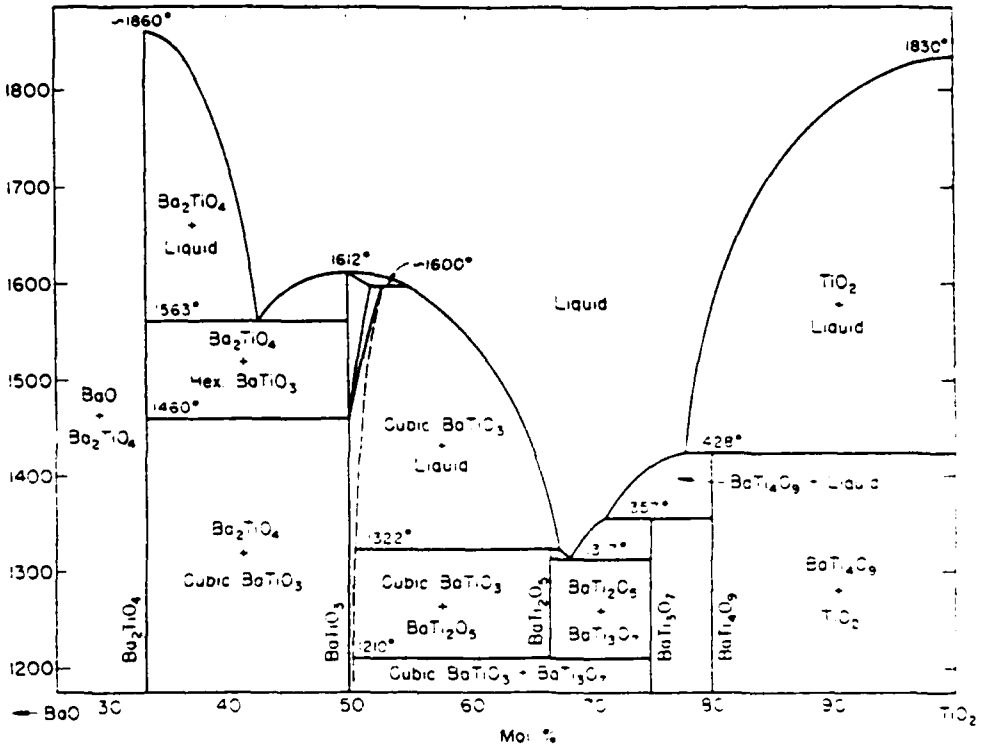

Fig. 7: BaO-TiO_2 phase diagram [16].

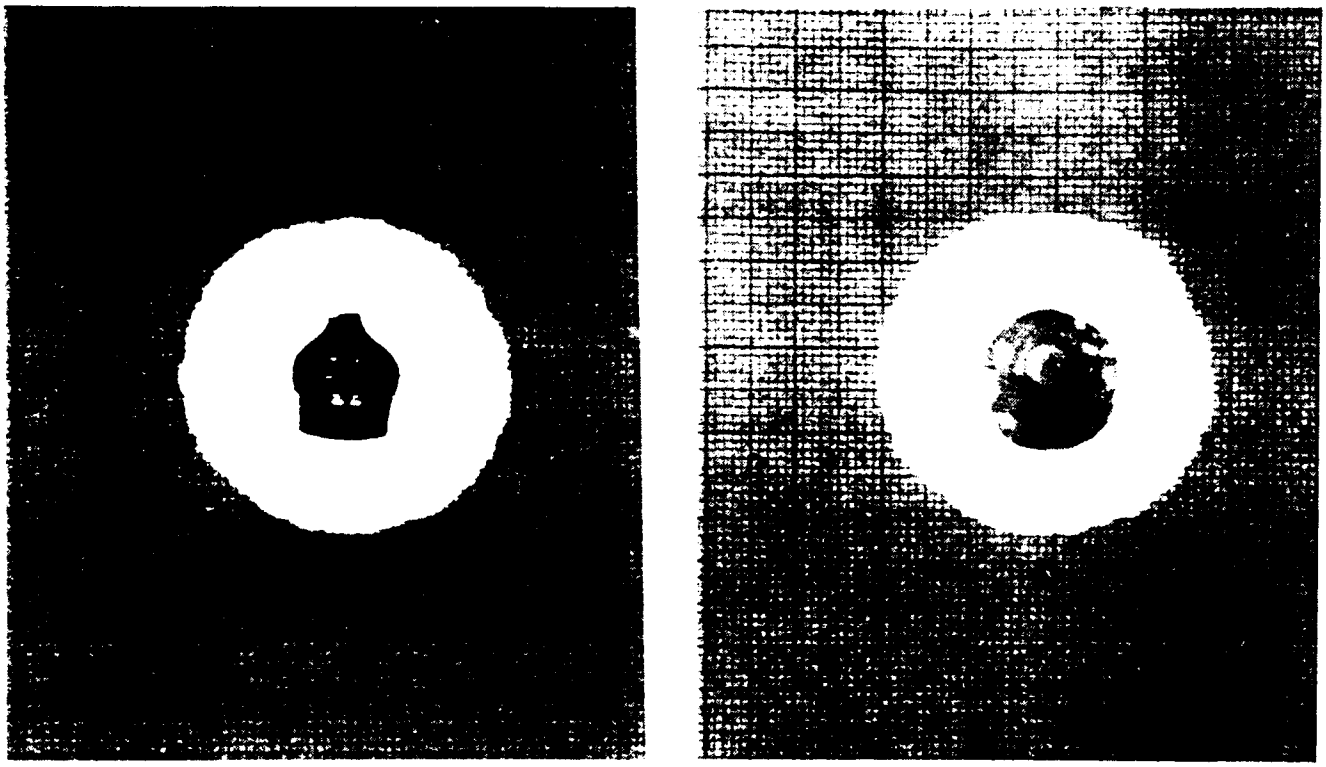

Fig. 8: Boule grown by top-seeded solution growth method with pulling from a melt of composition $Sr_{.12}Ba_{.88}TiO_3$ using SiC furnace (left - side view, right - top view) (mm scale).

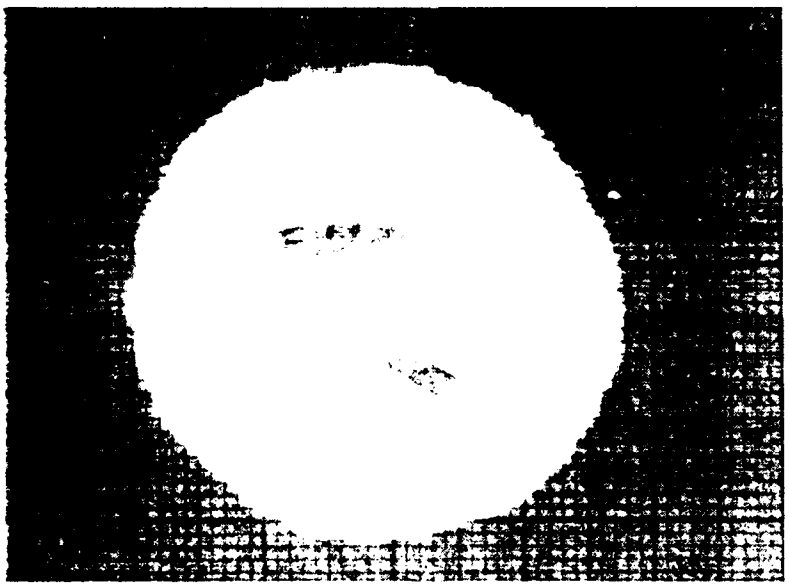

Fig. 9: Fabricated samples of $Sr_{.12}Ba_{.88}TiO_3$ from a boule grown from solution using RF indication heating.

Using RF induction heating and a modified Czochralski furnace, several single crystal boules of $Sr_xBa_{1-x}TiO_3$ large enough for property measurements were grown. Some samples fabricated for evaluation are shown in fig. 9. They contained a few defects, probably inclusions of TiO_2. Again, since the program was redirected at this point, none of the above crystals were actually evaluated.

B. Scandium Tantalate and Niobate

1. Introduction

Scandium orthotantalate $ScTaO_4$, as mentioned earlier, was recently reported by Zhong, et al. [4] to be a ferroelectric material with a Curie temperature of 7°C and a peak relative permittivity ε of around 7300. These properties make it of interest for application in devices operating at room temperature and which require a high value of ε.

The stable phase of $ScTaO_4$ is monoclinic with the wolframite structure, space group P2/c and lattice constants a = 4.807 Å, b = 5.662 Å, c = 5.112 Å, and β = 91°37' [17]. Its melting point has been reported as 2340°C [18] so that single crystal growth from the melt would be difficult by conventional techniques. Zhong et al. [4] grew 1 mm size crystals by the flux method and we have confirmed that slow cooling a solution of $ScTaO_4$ in the $PbO/PbF_2/B_2O_3$ flux they used yields small, transparent crystals of the appropriate phase.

The laser-heated pedestal growth (LHPG) method is particularily suited to the growth of high melting oxides such as $ScTaO_4$, since they can be melted relatively easily by a CO_2 laser beam and a crucible for the melt is not required. Since scandium compounds are currently very expensive because of their scarcity and their recent demand for use in crystalline and vitreous laser host applications, the small quantities of material needed for these experiments was a significant advantage.

2. Synthesis and Growth

In this program, $ScTaO_4$ was synthesized from equimolar quantities of powdered Sc_2O_3 and Ta_2O_5 by reactive hot pressing. The samples were mixed by agitation in isopropanol, dried and pressed using an Astro hot-pressing

furnace with graphite dies lined with boron nitride. Samples of about 90% of theoretical density (6.92 g cm^{-3}) were prepared by pressing for 4 h at 1350°C under 6000 psi pressure. X-ray diffraction analysis of these samples showed traces of unreacted Ta_2O_5, so heating for 12 h at 1200°C in oxygen was used to complete the reaction. The resulting samples were white, and x-ray diffraction analysis showed only the wolframite structure with lattice constants in agreement with ref. [17].

Single crystal were grown using a laser heater power of 20 W, and at pull rates of 0.5 - 1.0 mm/min. Bubbling in the molten zone was often observed and was attributed either to the presence of carbon from the hot-pressing furnace or to porosity of the source material. Since this bubbling made it difficult to grow a crystal of constant diameter, a 2-stage process was developed. In the first stage, a crystal was grown from the hot-pressed source material. This crystal was then used as the source rod and regrown to produce a high quality crystal of constant diameter. The melt was quite stable in the second stage, and optically clear, transparent crystals were produced as in the example shown in fig. 10. It was confirmed by optical pyrometry that the melting point of $ScTaO_4$ is about 2300°C, and that this compound appears to melt congruently.

When the single crystals grown by this method were ground and analyzed by x-ray powder diffraction techniques, they were found to have the tetragonal zircon structure rather than the room temperature wolframite phase. Cooling of the small diameter crystals to room temperature is fairly rapid in the laser-heated pedestal method, so metastable phase formation is not uncommon.

To verify that the zircon structure of $ScTaO_4$ is a metastable phase, sections of single crystals were heated to various temperatures, then cooled and again analyzed by x-ray diffraction. The temperature for the tetragonal monoclinic transition was found to be in the range 1400-1600°C.

Tetragonal $ScTaO_4$ (space group I4/amd) has not been reported previously but the structure is analogous to $ScVO_4$ which is also known to be ferroelectric [19]. Powder x-ray diffraction data for the tetragonal $ScTaO_4$ are

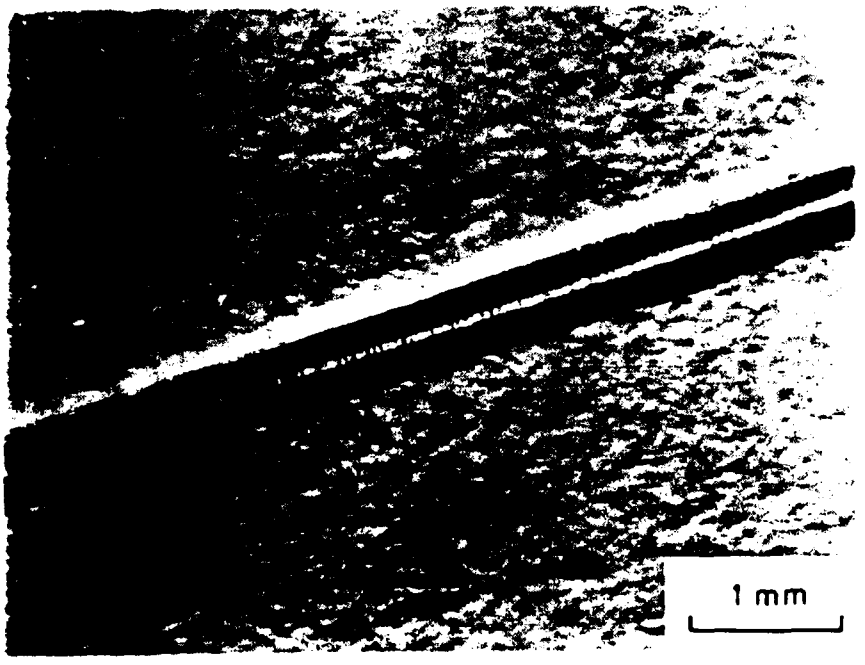

Fig. 10: Single crystal fiber of tetragonal $ScTaO_4$ grown by the laser-heated pedestal growth method.

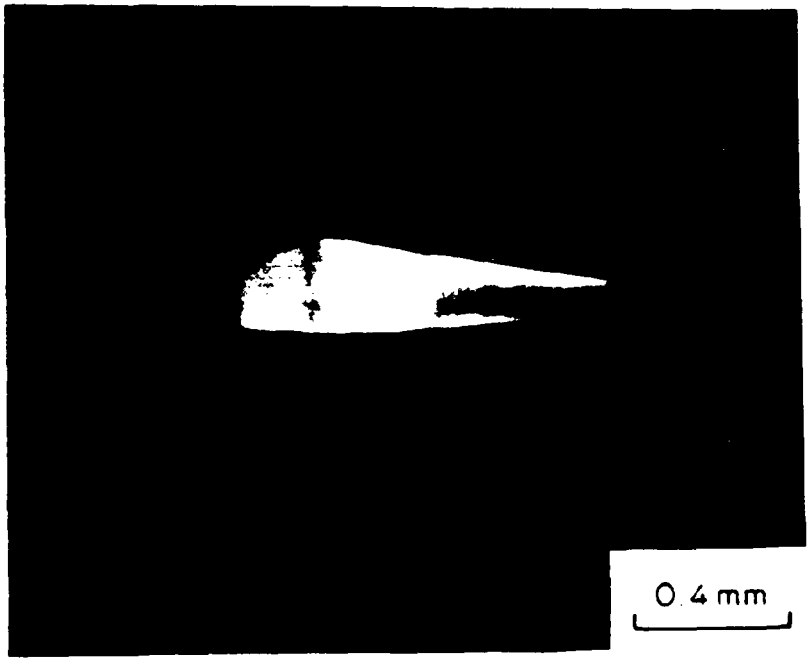

Fig. 11: Typical result of experiments aimed at fiber growth of $ScNbO_4$. Instability of the melt leads to diameter variations and polycrystallinity.

reported in table 1. The lattice parameters are a = 6731 ± 0.014 Å and c = 6.409 ± 0.020 Å. The theoretical density, 6.63 g cm^{-3}, is about 4% less than that of the wolframite phase.

Attempts were also made to grow crystals of the analogous compound $ScNbO_4$ by the same method. Scandium orthoniobate also has the monoclinic wolframite structure [20] with a = 4.807 Å, b = 5.453 Å, c = 5.094 Å, and β = 91°37'. $ScNbO_4$ was prepared by hot-pressing mixtures of Sc_2O_3 with Nb_2O_5, but cold-pressing of the powders followed by reaction sintering was found to be preferable for complete reaction. Small crystals grown by the LHPG method were found to retain the wolframite structure, but $ScNbO_4$ appears to melt incongruently as suggested by Vladimirova et.al [18]. Incongruently melting compounds can be crystallized by LHPG if the growth rate is reduced, but in the case of $ScNbO_4$ the melts were very unstable making controlled growth difficult. Unlike $ScTaO_4$, unstable melts were observed even during the second stage of the 2-stage processing.

Fig. 11 shows the result of a typical attempt to grow a $ScNbO_4$ crystal. The initial region, on the right of the photograph, is monocrystalline and relatively clear. As growth proceeded, it was difficult to control the fiber diameter, and eventually the crystal froze onto the source rod (a previously grown crystal), part of which can be seen at the extreme left (dark region). The resulting polycrystallinity and rapid cooling led to cracking. The section of source rod attached to the crystal shows the typical diameter variations found in material grown during the first stage from hot-pressed starting material.

Several attempts were also made to grow crystals of $ScNbO_4$ by the flux method. The literature suggests that rare earth niobate crystals can be grown from PbO/PbF_2 [21], PbF_2 [22], and Bi_2O_3/B_2O_3 [21] fluxes. In every case, however, we found that slow cooling from similar compositions yielded complex oxide crystals having a defect fluorite structure and containing Pb or Bi respectively, in addition to Sc and Nb. Some alternative novel flux, such as ScF_3, might be necessary to grow crystals of $ScNbO_4$.

TABLE 1

X-ray diffraction data for tetragonal $ScTaO_4$

d(Å)	I/I_0	hkl
3.333	15	020
3.129	75	002
2.605	15	112
2.365	7	220
2.074	10	301
1.919	100	222
1.754	15	132
1.741	5	123
1.670	3	040
1.601	10	004
1.498	15	240
1.410	50	233
1.370	5	242
1.214	3	152
1.187	5	440
1.151	2	044
1.109	4	442
1.083	10	352
1.063	3	260
1.045	3	116
1.021	4	154
0.995	3	361
0.959	45	444

III. FERROELECTRIC FLUORIDES

A. Introduction

For electro-optic applications, octahedrally coordinated ferroelectric oxide compounds are well suited and widely used. In comparison with the enormous number of ferroelectric oxides that have been discovered and studied [23], only a handful of structurally analogous halides have been discovered. Although most IR fluorides have low indices of refraction, true ferroelectric fluorides would be expected to have significantly higher values, particularly those which have Curie temperatures not too far above room temperature.

A new class of true ferroelectric fluorides was discovered by Professor Hagenmuller's group at the University of Bordeaux, France [5]. So far this group has identified nine compounds from the $A^{II}B^{III}F_5$ group which appear to be true ferroelectrics: $SrAlF_5$, $SrGaF_5$, $SrCrF_5$, $BaTiF_5$, $BaVF_5$, $BaFeF_5$, $PbAlF_5$, $PbGaF_5$, and $EuAlF_5$. The phase transition temperatures are reported to be a function of the A^{++} and B^{+++} ionic radii. For $SrAlF_5$ it is reported to be 685°K.

We originally proposed to select several promising candidates from this group such as $BaTiF_5$, $PbAlF_5$ and $PbGaF_5$, study their phase equilibria, and synthesize them in single crystal form for property evalution. If the results were promising, we planned to look at the formation of solid solutions as a way of tailoring the material properties. Ternary fluorides containing binary phases which are volatile and have a large density difference, such as AlF_3 and PbF_2 for example, are nontrivial to grow in single crystal form for reasons explained later.

1. Theory of Ferroelectricity in Fluorides

Soft modes depend strongly on anion polarizability [23]. More than 98% of ferroelectric and antiferroelectric substances are chalcogenides, mainly oxides as mentioned previously. A linear chain model may be used to describe the lattice vibrations in terms of cation and anion masses and coupling constants (see, for example, ref. 23) but we have not seen these models applied to explain dispersion curves of transverse acoustic and ferroelectric modes in fluorides.

The polarizability of O^{2-} has been described by Watson [24] who introduced an electrostatic model in which the $^{+}2$ charge on surrounding cations is uniformly distributed over a sphere. The depth of the potential well is put equal to the Madelung potential at the O^{2-} site and this defines the Watson radius R_W, which is proportional to the lattice constant. The dependence of the polarizability α on R is found to be qualitatively different for O^{2-} and F^- [23] even though these are iso-electronic ions (see fig. 12). In the limit $R_W \to \infty$, the polarizability of F^- is found to reach the free ion value, whereas that of O^{2-} diverges. In some oxides, e.g. perovskites, the oxygen ion exhibits a strongly anisotropic charge distribution whch leads to enhancement of the volume dependence of αN.

Ferroelectricity has been established in the $BaMF_4$ family of compounds when M = Mg, Co, Ni, and Zn [25]. Good single crystals were available for these studies. The reversal of polarity in these materials has been explained [26] by a model in which four fluorine ions lying on a mirror plane passing through the M atom rotate by 1.1 Å about M and displace the Ba^{2+} ion by 0.67 Å along the polar axis relative to the M positions. The absence of a ferroelectric transition when M is Mn or Fe was explained on the basis that rather large changes in M-M and M-F distances would be required for this switching to occur. Fairly detailed structural data is available on these materials. The $BaMF_4$ materials are classified as two-dimensional ferroelectrics.

2. The Alkaline Earth - Group III Fluorides

As mentioned above, the $SrAlF_5$ family of materials was investigated by Ravez et al. [5,6]. $SrAlF_5$ is tetragonal, space group I4 with unit cell dimensions a = 14.04 Å and c = 7.17 Å. The arrangement of atoms is shown in fig. 13; chains of corner-sharing AlF_6 octahedra alternate with parallel chains of corner-sharing octahedra that simultaneously share corners with single octahedra [7]. The spontaneous polarization was estimated from two simple atomic models to be 48 x $10^{-2}cm^{-2}$ and 9 x $10^{-2}cm^{-2}$ respectively.

Measurements were made on polycrystalline discs fired in sealed gold tubes under nitrogen at 1025 K [5]. A single crystal was available only of

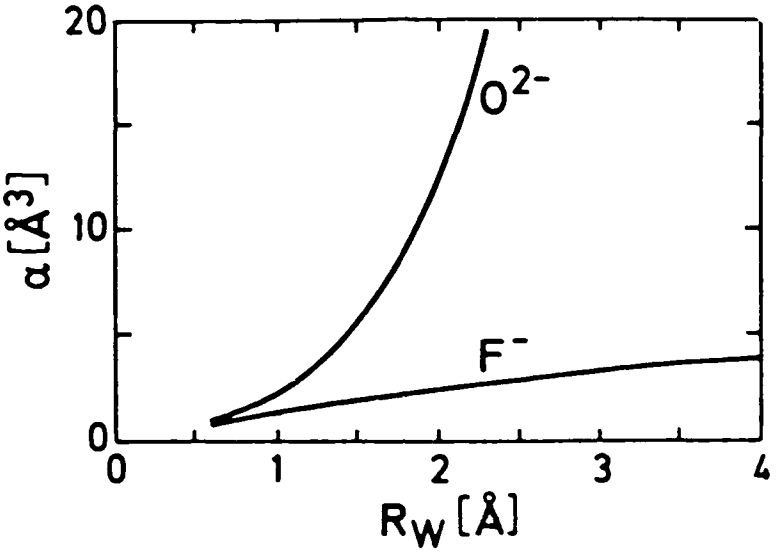

Fig. 12: Polarizabilities of F^- and O^{2-} ions as a function of the Watson radius [23].

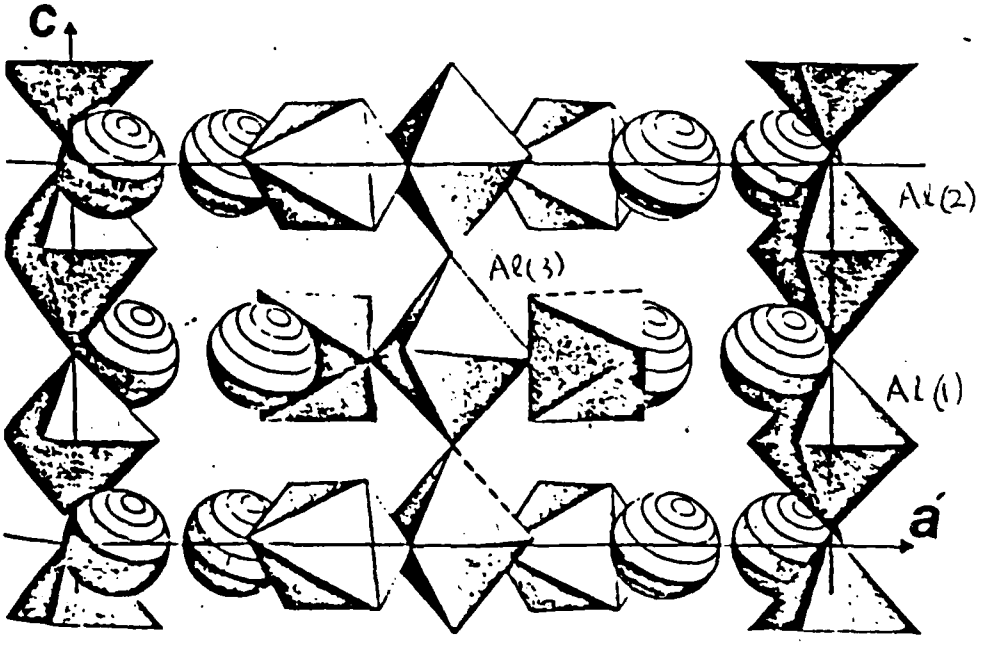

Fig. 13: Arrangement of two kinds of octahedral chains in $SrAlF_4$ [7]. The figure shows half the unit cell, the remaining half being obtained by a translation of $\frac{a}{2}$ and $\frac{c}{2}$. The spheres are Sr^{2+}.

$SrAlF_5$ itself and colorless crystals up to 2.5 mm in size were cut from boules grown by the vertical Bridgman method and various experimental tests for ferroelectricity performed [6]. Second harmonic generation was demonstrated on polycrystalline material, with an efficiency close to that of quartz. The piezoelectric d_{33} coefficient was measured on crystal samples by applying a static stress on (001) surfaces and measuring the charge generated. The maximum value was $d_{33} = 0.3 \times 10^{-12} CN^{-1}$, and there was a distribution of values attributed to a variable domain structure. Attempts at poling the materials at room temperature with fields up to 1.3 $kVmm^{-1}$ were unsuccessful. A specific heat maximum was observed at 695°K. The temperature dependence of the dielectric constant, ε_1, was measured on polycrystalline discs and found to exhibit a maximum of 22 at about 715°K, at 1 KH_z. Ionic conduction was suspected at the higher temperatures. Reversal of the spontaneous polarization was not demonstrated in any sample.

In addition to $SrAlF_5$, ceramic samples of $SrCrF_5$, $SrGaF_5$, $BaTiF_5$, $BaVF_5$, $BaFeF_5$, $PbAlF_5$, $PbGaF_5$, and $EuAlF_5$ were also prepared [5]. Anomalies in the dielectric constant behavior with temperature were generally observed. The dielectric constant of $PbAlF_5$ had a peak value around 5000. Curie temperature, T_c, for these compounds were in the range from 495°K to 715°K. The value of T_c was the same (585 ± 10°K) for $PbAlF_5$ and $PbGaF_5$, but no attempt was made to explain the range of values in terms of bonding parameters.

In 1969, Shore and Wanklyn [27] studied the PbF_2-AlF_3 phase diagram and found only one phase, $Pb_3Al_2F_{12}$, not the $PbAlF_5$ phase reported above. They found $Pb_3Al_2F_{12}$ to have a space group of I4/m with lattice constants of a = 14.23 Å, c = 7.20 Å and space group I4/m. Recently Abrahams et al. [28] reported on the ferroelectric behavior of related Pb compounds of the type $Pb_3M_2F_{12}$ (M = Fe, Ga, Ti, V).

Samples of $Pb_3M_2F_{12}$ were prepared br Abrahams et al.[28] by reacting PbF_2 and MF_3 in a sealed gold tube after intimate mixing. Values of d_{33} were measured by a laser illumination method and large specific heat anomalies were observed by differential scanning calorimetry. T_c values ranged from

550°K for $Pb_3Cr_2F_{12}$ to 740°K for $Pb_3Fe_2F_{12}$. Large peaks in the dielectric constant versus temperature plots were observed at similar temperatures (560°K for the Cr compound and 725°K for the Fe). Maximum values of ε_1 were from 200 - 300. As in the case of $SrAlF_5$ and other materials with the 1-1-5 stoichiometry, a convincing demonstration of ferroelectricity by reversal of the spontaneous polarization was not achieved since suitable, high purity single crystals were not available.

3. Purification

Purity is of extreme importance in ferroelectrics since property measurements in the neighborhood of ferroelectric phase transitions are very sensitive to impurities and to crystal defects. As an example of the importance attached to crystal perfection in some laboratories, the group of K. A. Muller at the IBM Zurich Research Laboratory spent over 10 years in attempting to prepare very pure and perfect crystals of $GdAlO_3$ and $SrTiO_3$. The crystal growth effort led to improvements in the flame fusion technique [29] and to a very major advance in flux growth—the accelerated crucible rotation technique [30]. Crystals of $GdAlO_3$ up to 120 g in weight were eventually grown by the flux method, with dislocation densities below 10 cm^{-2}.

Our own experience with crystal growth from melts in the PbF_2/AlF_3 system as described later in this report has emphasized the need for purification of the starting materials. Fluorides are prone to hydrolysis, leading to contamination by oxide, hydroxide and oxyfluoride impurities which are often very difficult to remove. The open structure of AlF_3 allows water molecules to enter readily, forming hydrates from which water can be removed only with difficulty. When heated, some loss of HF and formation of Al_2O_3 occurs, especially if the hydrate is heated rapidly above 300°C. Attempts to prepare anhydrous AlF_3 usually depended on heating the oxide in HF, but the reaction

$$Al_2O_3 + 6HF \rightarrow 2AlF_3 + 3H_2O$$

usually does not proceed completely.

Rolin [31] has described a procedure for purification of AlF_3 by vacuum sublimation. The trihydrate was first dehydrated by slow heating up to 400°C, with the sublimation being effected by rf heating of the sample in a graphite crucible. The temperature was raised to 1200°C and the 250 g charge collected by condensation on the graphite wall at about 900°C. The distilled AlF_3 prepared in this way still contained about 0.1% of Al_2O_3.

A method for purification of oxygen-contaminated fluorides was described by Warshaw and Jackson [32]. This was based on the passage of HF in an argon carrier gas over the molten fluoride. In the example of LaF_3, 0.5 wt% of PbF_2 was added to the prereacted charge to compensate for surface moisture absorption. However, as Chernevskaya and Korneva [33] have pointed out, gaseous HF is not the optimum fluorinating gas because of thermodynamic considerations [34] and because of its corrosive nature. They introduced tetrafluorethylene directly inside the crucible containing a CaF_2 charge and obtained crystals of high transparency.

Zone melting is an alternative procedure which may be successfully applied to fluoride purification in some cases. The application to KCl was reviewed by Warren [35], who claimed that impurity levels could be reduced below 10 ppb. Results with LiF and some other fluorides were not that successful.

Pastor and Arita [36] have stressed the importance of a reactive gas atmosphere during the crystal growth of halides. They grew alkali halide crystals with high transmission coefficients but commented that HF is the least effective agent among the hydrogen halide gases. In a later study [37] they used mixtures of CF_4 with HF, which caused further improvements in optical transparency compared with HF alone. Next [38], they compared CF_4 with C_2F_4 for their effectiveness in removing oxides and moisture from fluorides. The C_2F_4 was produced by depolymerization of teflon $(C_2F_4)_n$, and optimum temperatures for this depolymerization reaction were determined. In the final paper of this series [39], SF_6, CF_4, and BF_3 were compared as gas-phase reactants for the crystal growth of alkaline earth fluorides. All three are corrosive to carbon. Transmission curves were compared for SrF_2 crystals

grown under these 3 atmospheres and the BF_3 was found to give the best results.

4. Fluoride Crystal Growth

As mentioned in the previous section, the crystal growth of metal fluorides requires some specialized techniques which prevent the formation of oxides and oxyfluorides. Some materials of course are more problematic than others. Many methods have been used to grow a variety of binary and ternary fluorides successfully including flux growth from slowly-cooled melts, some containing ammonium fluoride, in platinum containers with tightly-fitting lids [40], vertical Bridgman growth in platinum containers sealed under dry argon [41], vertical Bridgman growth in graphite crucibles after heat-treatment in reactive atmospheres containing gaseous HF, CF_4, C_2F_4 from decomposing teflon, SF_6, and BF_3 [36-39], horizontal Bridgman, zone melting, and Czochralski growth of crystals pulled under atmospheres containing HF and F_2 [41,42]. Because the lead aluminum fluoride phase we were trying to grow melts and probably vaporizes incongruently, a modified vertical Bridgman growth technique seemed the most appropriate method for the growth of large crystals because of the small surface to volume ratios involved. It was the only method used in this program except for some brief attempts at zone melting.

B. Results and Discussion

1. Synthesis and Growth of $SrAlF_5$

When SrF_2 and AlF_3 powders are mixed together and heated, the AlF_3 evaporates strongly at temperatures well below the melting point of either constituent. We found it necessary to synthesize the $SrAlF_5$ by co-precipitating the constituents as a very fine, intimate mixture. In the method we used, aluminum nitrate was vacuum dried, weighed and dissolved in DI water. This solution was mixed with an equimolar solution of strontium nitrate, and 48% hydrofluoric acid solution was added to precipitate the fluorides from a stirred solution. The precipitate was dried in air at 80°C for about fifteen hours and was then heated in a flowing hydrogen fluoride/argon stream at 950°C for two hours to remove traces of moisture. The weight loss during this heat treatment was typically 3%.

$SrAlF_5$ was successfully grown using our pre-existing fluoride growth equipment. These crystals were grown by the vertical Bridgman method in graphite crucibles with a conical bottom and a 1" long capillary section where nucleation and growth was initiated. The lowering rate during growth was normally 1 mm/hr and the mole fraction of excess aluminum fluoride in the starting melt composition was varied from 10% to 25%. Many of the crystals which were grown were very clear throughout most of their volume, although milky, white regions were sometimes observed in the last few mm. The major problem was cracking, as illustrated in the photograph in fig. 14, which prevented the growth of clear crystals several cm^3 in size. The largest crack-free specimens from $\approx$ 40g charges were about 3-5 g in weight. Polished crystals were very clear in transmitted light although the surfaces were etched quite rapidly by atmospheric attack. Boules had a preference for growth along the c-axis although major variations occurred from one run to another.

The largest crystal grown to date (about 11x5x5 mm [see fig. 15]), was sent to Dr. M. Klein at Hughes Research laboratories for measurement at mm wave frequencies (96 MHz). The dielectric constant was found to be about 9, a little lower than the reported DC value [6], but the losses were relatively low. The maximum value of the relative permittivity quoted by Abrahams et. al [6] was 23, for an unspecified orientation. The low loss and the apparently weak frequency dependence of the dielectric constant were considered important advantages which may also apply to similar materials.

2. The PbF_2-AlF_3 System

a. Previous Work

$PbAlF_5$ was reported to have a DC permittivity of 4800 at its ferroelectric transition temperature of 312°C [6], much higher than that of $SrAlF_5$. The phase relationships in the PbF_2-AlF_3 system were studied by two groups [27,43] and their conclusions are in major disagreement. Ravez and Dumora [43] report the existence of three intermediate phases: $PbAl_2F_8$, $PbAlF_5$, and $Pb_9Al_2F_{24}$. All three were found by sintering powders in sealed gold tubes at temperatures below their melting or decomposition temperatures,

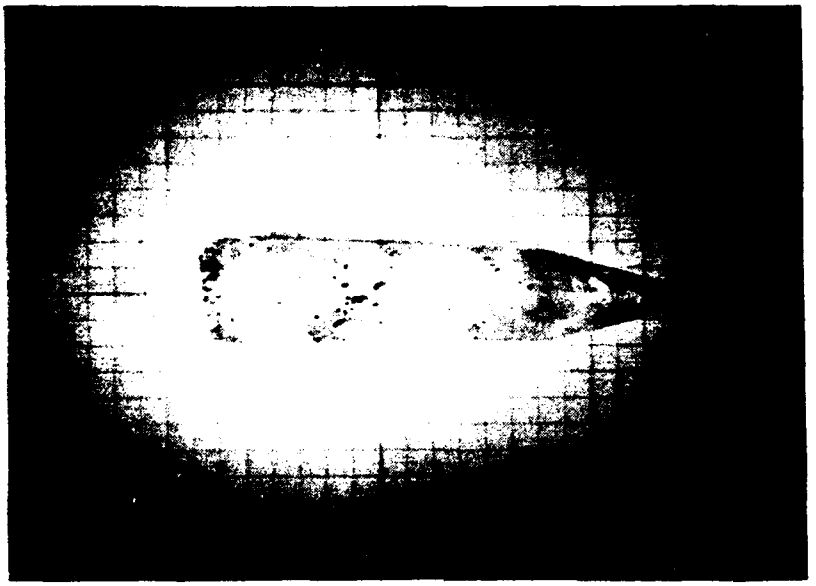

Fig. 14: $SrAlF_5$ boule grown by the Bridgman method (inch scale). The boule is single crystal but cracked.

Fig. 15: Single crystal of $SrAlF_5$ cut from larger boule (#16) (inch scale).

which were reported to be 614, 618, and 560°C respectively. $PbAlF_5$ was reported to have a tetragonal structure (space group I4C) with a = 14.19 and c = 7.280 Å, and with a density of 5.91 g/cc. The existence of a compound with this stoichiometry however, was refuted by the work of Shore & Wanklyn [27]. They performed experiments in which melts of various PbF_2-AlF_3 compositions were slow-cooled from the liquid phase. The only intermediate compound they found was $Pb_3Al_2F_{12}$ which is tetragonal (space group I4/m), has a density of 6.47 g/cc, and lattice constants of a = 14.23, and c = 7.20 Å. Clearly the $Pb_3Al_2F_{12}$ phase of [27] is closely related to the $PbAlF_5$ of [43]. Both structures belong to ferroelectric classes and either or both could be of interest.

An analysis of these two research efforts suggested that different purity and processing conditions may have led to the conflicting results. Kinetic factors may also be very important. Shore & Wanklyn's relatively fast cooling rates were quite different from Ravez et. al's long term (near equilibrium) annealing experiments and the former's results may be consistent with metastable conditions. It was one of the goals of this program to resolve this question as well as to prepare high quality crystals of the appropriate phase or phases so that the ferroelectric properties could be accurately measured. Our approach involved: a) careful purification of the starting material, b) controlled synthesis and phase equilibria analysis, c) the growth of cm size high quality single crystal samples, and d) characterization of physical and chemical properties of these crystals including their ferroelectric properties. Much progress has been made in this area as will be discussed later.

The type of phase diagram expected from the Ravez and Dumora data is shown in fig. 16 while a very different phase diagram was proposed by Shore and Wanklyn (fig. 17) based on DTA data. Our own preliminary DTA results are consistent with the phase diagram shown by Shore and Wanklyn, although we have found evidence for the $Pb_9Al_2F_{24}$ phase reported by Ravez. We have also found some preliminary evidence for the existence of the $PbAlF_5$ phase in long term annealing experiments at temperatures below 614°C in sealed tubes, but

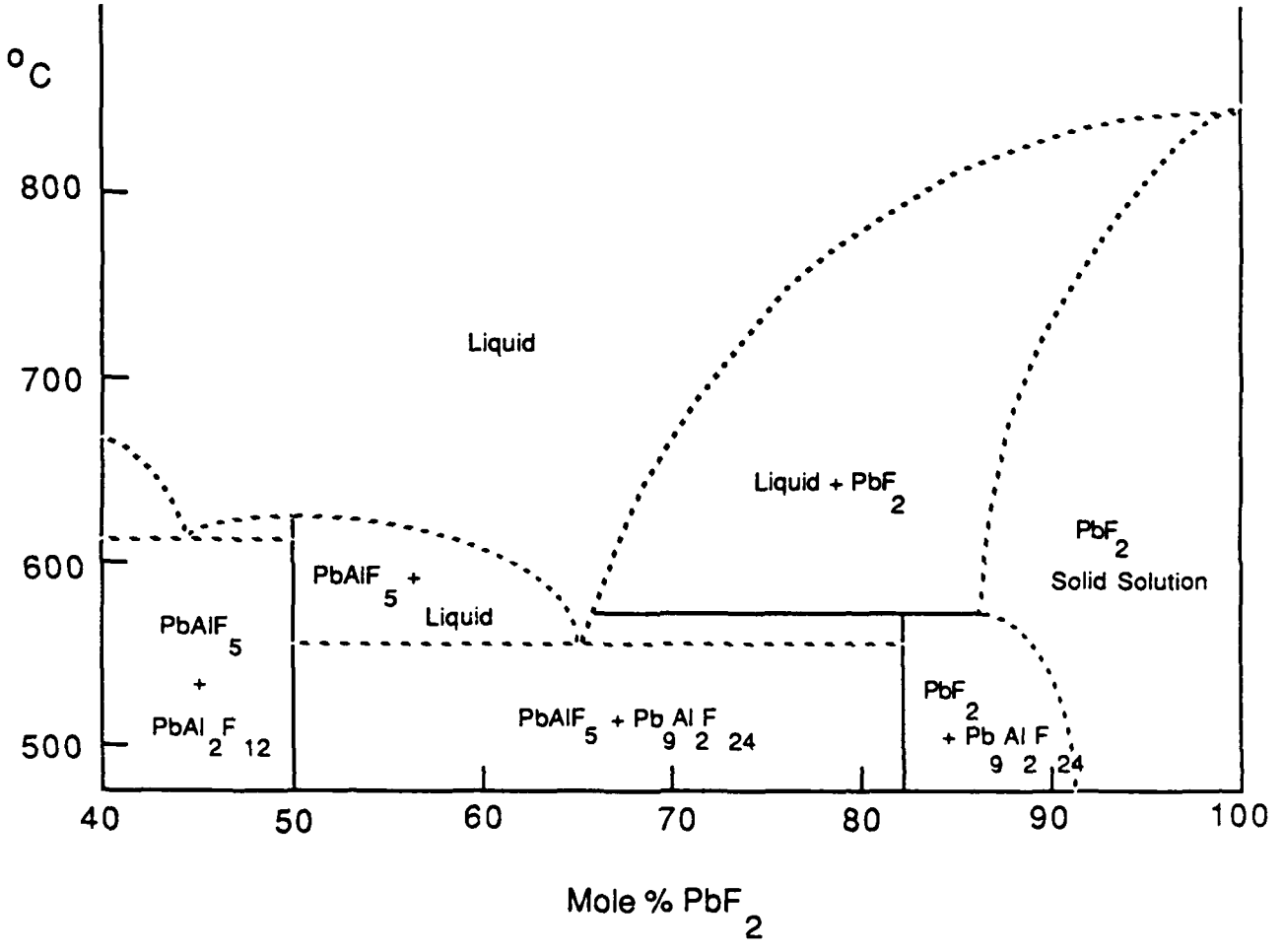

Fig. 16: Phase diagram of PbF_2-AlF_3 system constructed from data of Ravez and Dumova [43]

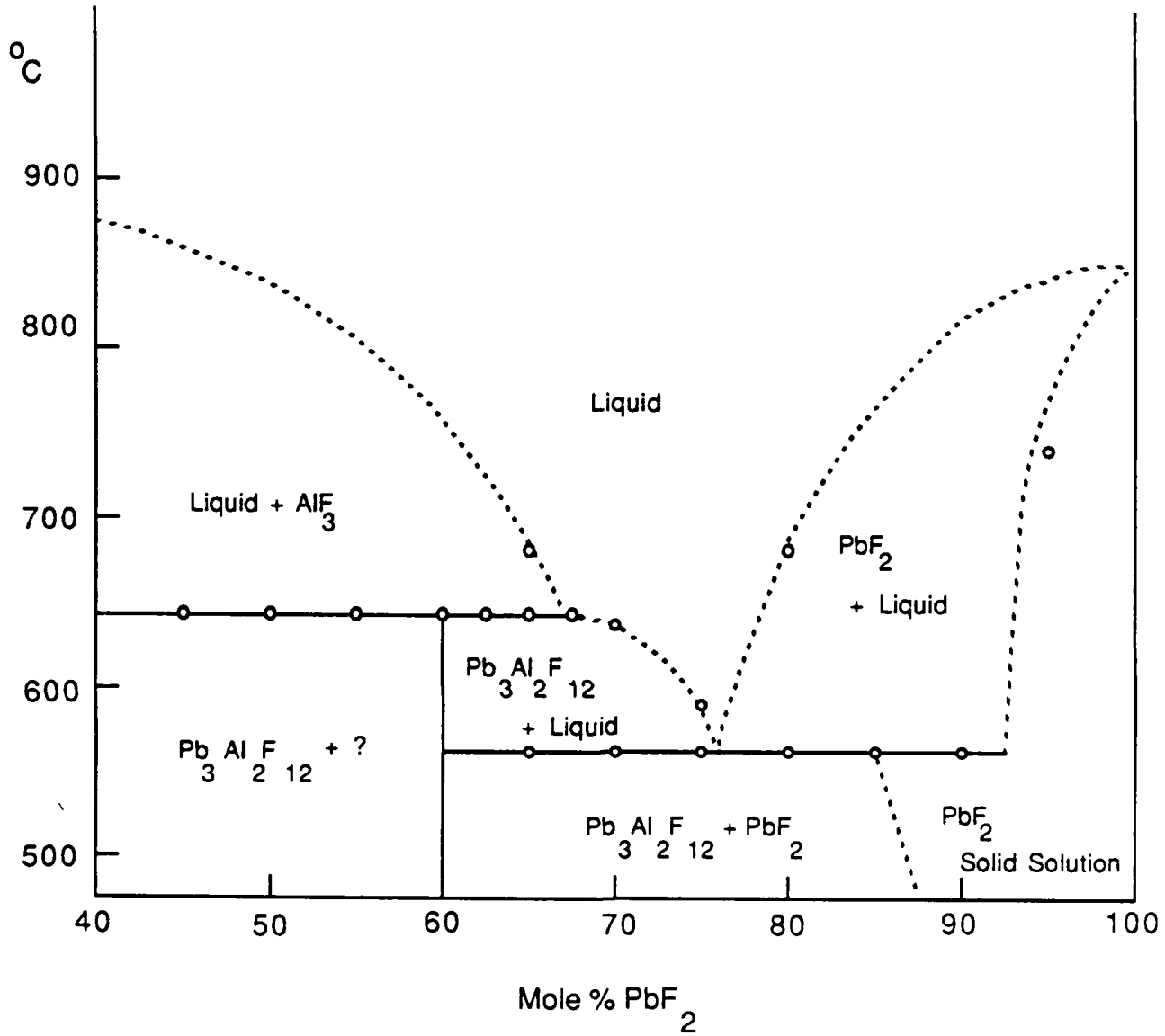

Fig. 17: Phase diagram of PbF_2-AlF_3 system constructed from data of Shore and Wanklyn [27].

in crystal growth experiments where non-equilibrium conditions may exist, the $Pb_3Al_2F_{12}$ phase seems to predominate. X-ray diffraction and electron microprobe analysis have not yet given conclusive results but at the present time the existence of the $Pb_3Al_2F_{12}$ phase seems likely, at least under certain (normal) solidification conditions. It is still planned to verify the existence of the $PbAlF_5$ phase conclusively in future studies.

A careful comparison between the $BaFeF_5$ and $Sr_3Fe_2F_{12}$ structures, which would be analogous to the structures of $PbAlF_5$ and $Pb_3Al_2F_{12}$ respectively, was presented by Ravez et al. [44]. Both structures are tetragonal and contain a similar framework of interlocking iron fluoride octahedra, the lattice constants being related by the ratios: $a_{Sr_3Fe_2F_{12}} \cong \sqrt{2}aBaFeF_5$, and $c_{Sr_3Fe_2F_{12}} \cong 2cBaFeF_5$. For $PbAlF_5$ or $Pb_3Al_2F_{12}$ aluminum fluoride octahedra would provide the structural framework. Projections of the $BaFeF_5$ and $Sr_3Fe_2F_{12}$ structures on the xy plane are shown in fig. 18a. Here one can see the close similarity of the two structures. These consist of chains made up of FeF_6 octahedra and the simple rearrangement of the divalent ions and corner-shared octahedra necessary for conversion between the two, is shown in fig. 18b. Since these structures are so similar, discrimination between the two is difficult on the basis of x-ray powder diffraction data alone. In systems such as PbF_2-GaF_3, BaF_2-TiF_3, BaF_2-VG_3, and BaF_2-FeF_3, phases of both stoichiometries have been found.

b. Synthesis and Purification

One cannot coprecipitate lead fluoride with aluminum fluoride from the nitrates as we did for strontium aluminum fluoride, since lead nitrate precipitates from HF solutions instead of forming the fluorides. It was necessary, therefore, to synthesize aluminum and lead fluoride powders directly by fusion under hydrogen fluoride. Both PbF_2 and AlF_3 have substantial vapor pressures at the temperatures required for reaction, so changes in stoichiometry will occur during reaction or crystal growth under a flowing atmosphere. Another complication is that mass spectrographic analysis of lead fluoride evaporation [45] indicates that incongruent vaporization occurs

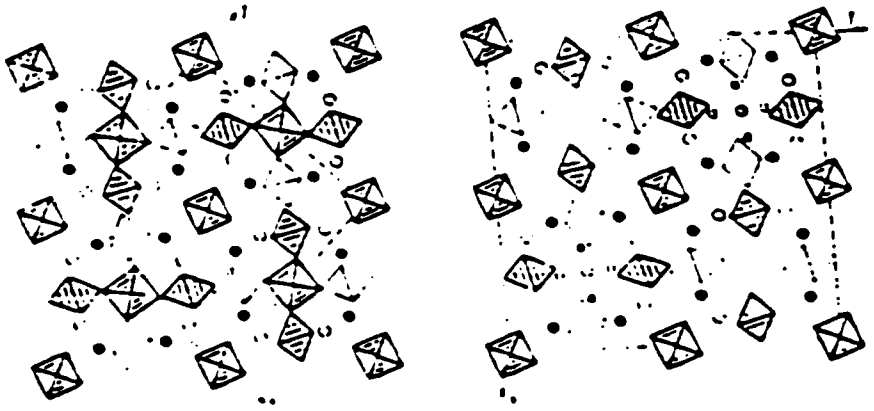

Fig. 18(a): Projections of the $BaFeF_5$ an $Sr_3Fe_2F_{12}$ structure on the xy plane.

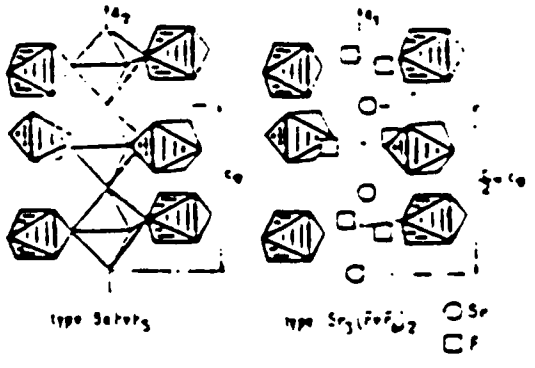

Fig. 18(b): Mode of conversion from $BaFeF_5$ to $Sr_3Fe_2F_{12}$ structure type.

in an inert environment. This agrees with our experience thus far, having found in various stages of synthesis and crystal growth the presence of metallic lead. Some of the lead formed may also have been due to contamination problems.

The free lead formation, besides indicating a detrimental change in melt composition which complicates the growth of high quality inclusion-free crystals, also represents a more practical problem; the forming of low-melting alloys with most metals. Generally, fluorides at elevated temperatures are contained in graphite or platinum, since other materials will be severely attacked. Platinum-lead alloy formation will destroy the integrity of the synthesis and growth containers, so until free Pb formation is completely eliminated, the only safe containers are graphite.

The Pb inclusions led us to make rather extensive thermodynamic calculations in order to determine the probable reactions which can take place between the fluoride starting materials and their impurities, the gaseous atmosphere used, and the furnace components, in particular the graphite reaction tube. The ratio of the water vapor pressure to the HF pressure determines whether the fluorides will be converted to oxides or hydroxides, or vice versa. The ratio of the hydrogen pressure to the HF pressure will determine whether the fluorides are reduced to their metallic elements or not. The thermodynamic calculations also indicated that aluminum fluoride is much less likely to be reduced and much more likely to be oxidized than the lead fluoride.

There are several mechanisms by which metallic Pb can be produced including water vapor contamination and incongruent volatilization processes.

The most likely source of contamination is water. Aluminum fluoride is hydroscopic and will hold water tenaciously. Water can also be released from the furnace walls, particularly if the furnace tube is made from porous graphite which has not been vacuum-baked. Any water released at elevated temperature can then react with metals or graphite to produce gaseous hydrogen, which can then reduce PbF_2 by the reaction:

$$PbF_2 + H_2 = Pb + 2\ HF$$

Using an HF atmosphere forces the reaction to the left, preventing decomposition of the PbF_2. An HF atmosphere may also discourage oxygen incorporation from water adsorbed onto the surface of the starting material by the reaction:

$$PbF_2 + H_2O = PbO + 2\ HF$$

It is also possible that pure materials could vaporize incongruently. AlF_3 sublimes to form a gas of AlF_3 and Al_2F_6 molecules, so the evaporation of AlF_3 will probably not move the melt off the PbF_2-AlF_3 pseudobinary phase diagram. This is not the case for evaporation of PbF_2 according to Kmbov et al. [45]. From experimental data, they found that the vapor composition over PbF_2 at 988 K was 66% PbF_4, 25% Pb and 2% PbF. The value they derived for the partial pressure of Pb over the PbF_2 melt is greater than that indicated by the CRC handbook for Pb vapor over pure molten Pb. Thus they are describing a process of evaporation of PbF_2 which leads to volatile PbF and PbF_4 gases, and the condensation of Pb liquid droplets. As the heavy Pb droplets eventually fall into the melt, the melt becomes Pb-rich.

An HF environment would discourage Pb enrichment of the melt in this case by reacting with the gaseous Pb to form PbF, then PbF_2 before it had a chance to condense into Pb droplets.

Potential reactions in the synthesis system which could be important include:

A. Reduction Reactions from Oxides

1. $Al_2O_3 + 3C = 2Al + 3CO$
2. $PbO + C = Pb + CO$

B. H_2O Erosion/Contamination Reactions

1. $2AlF_3 + 3H_2O = Al_2O_3 + 6HF$ forward reaction favored
2. $PbF_2 + H_2O = PbO + 2HF$ reverse reaction favored
3. $C + H_2O = CO + H_2$

Some other findings included:

A. Routes to Pb contamination at 1200°K:

1. $P_{H_2O}/P^2_{HF} > 40$ leading to the formation of molten PbO, which will then reduce to Pb if it comes in contact with graphite.

2. $P_{H_2}/P_{HF} > 5 \times 10^{-18}$ allowing PbF_2 to reduce directly to Pb + HF. Since the natural composition of the atmosphere is 0.5 ppm (5×10^{-7}) H_2 which diffuses easily through most materials, slow decomposition of the PbF_2 by this route is hard to avoid. Breakdown of H_2O to H_2 by the hot Ti used in the Argon purification system or graphite can considerably expedite this process.

B. Oxidation Reactions at 1200°C:

1. As mentioned above, $PbF_2 \rightarrow PbO$ for $P_{H_2O}/P^2_{HF} > 40$.
2. $AlF_3 \rightarrow Al_2O_3$ for $P_{H_2O}/P^2_{HF} > 0.4$, although the kinetics will be more sluggish since both are in the solid phase.
3. The presence of O_2 by itself should not lead to Al_2O_3 or PbO formation, although oxygen is likely to be soluble in the fluorides.
4. At all elevated temperatures: $3PbO + 2\ AlF_3 \rightarrow Al_2O_3 + 3PbF_2$ is thermodynamically favored.

C. Action of Ti Furnace:

1. Excellent way to remove oxygen from Ar.
2. Decomposes H_2O to TiO and H_2.
3. Cooler parts of furnace can lower H_2 to ppm range if Ti hasn't been covered with oxide.

D. Problems with the Container Materials we have used:

1. Nickel furnace tube unsatisfactory since HF atmosphere at the high temperatures needed for $Pb_3Al_3F_{12}$ produced NiF_2 and H_2.
2. Platinum doesn't tolerate contact with liquid Pb.
3. Our graphite tubes are intrinsically more porous than we had realized.
4. Without a guard check valve, backflow of H_2O into the HF gas cylinder will occur.

E. Materials Purification at 1200°K:

1. For $P_{H_2O}/P^2_{HF} < 0.4$, oxides of Pb and Al should be fluorinated.

2. Free lead is hard to get rid of by fluorination. Would need $P_{H_2}/P^2_{HF} < 5 \times 10^{-18}$ to fluorinate it.
3. Sublimation can be used to separate the fluorides from Pb and Al_2O_3 which are significantly less volatile. Heating under vacuum will also drive off hydroxides, excess water, and other more volatile impurities. PbO unfortunately has similar volatility as AlF_3 and PbF_2.

Given the above considerations, the following steps should be taken to get rid of the free Pb: a) contamination of the starting materials with adsorbed water must be carefully avoided, b) furnace components should be baked out before use, and c) an HF atmosphere is preferable to an Ar atmosphere for fluoride processing at high temperatures but after heating in HF to the synthesis or growth temperature, argon can be used successfully.

After considering the system thermodynamics as described above, we made several significant improvements to our experimental procedures and apparatus. We started by improving our handling of the starting material powders to minimize the adsorption of water on their surfaces. We obtained a much better glove box for storage and handling of our materials. We also now transport our materials from the glove box to furnace in sealed bags filled with inert gas.

We have also greatly improved our hydrofluorination furnace (fig. 19 a&b). Since our graphite reactor tube was somewhat porous to begin with and became more porous when brought into contact with water or oxygen at elevated temperature, we had to provide an inert atmosphere on the outside to prevent contaminants from diffusing through it from the ambient atmosphere. A nickel sleeve with a water-cooled O-ring seal was placed around the graphite tube and purified argon, at an overpressure of around 100 mm Hg, was passed between the Ni sleeve and the graphite through a slotted brass conduction spacer. The gas lines to the furnace were also modified so that the interior of the graphite tube could be flushed with purified argon before and after HF treatment. The argon was purified by passing it over titanium shavings at a range of temperatures so that oxygen, hydrogen and water vapor were all

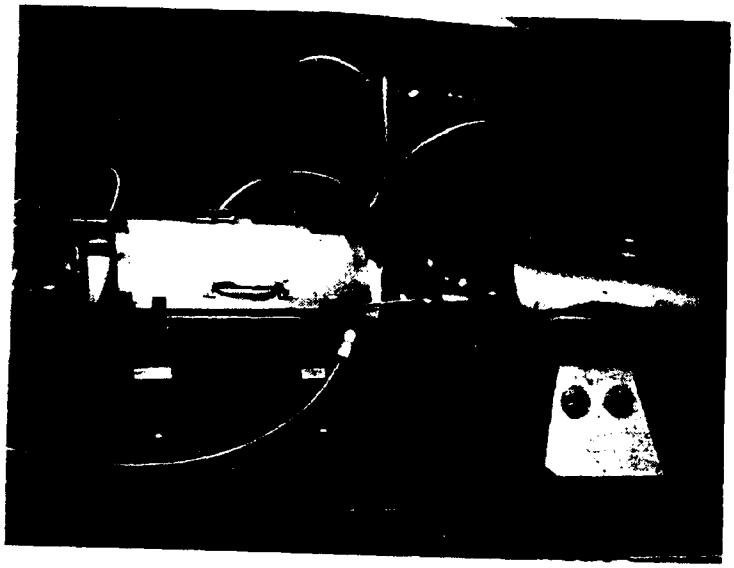

Fig. 19(a): Photograh of hydrofluorination furnace (left) and Ar purification furnace (right). The HF tank and exhaust bubblers are in the rear.

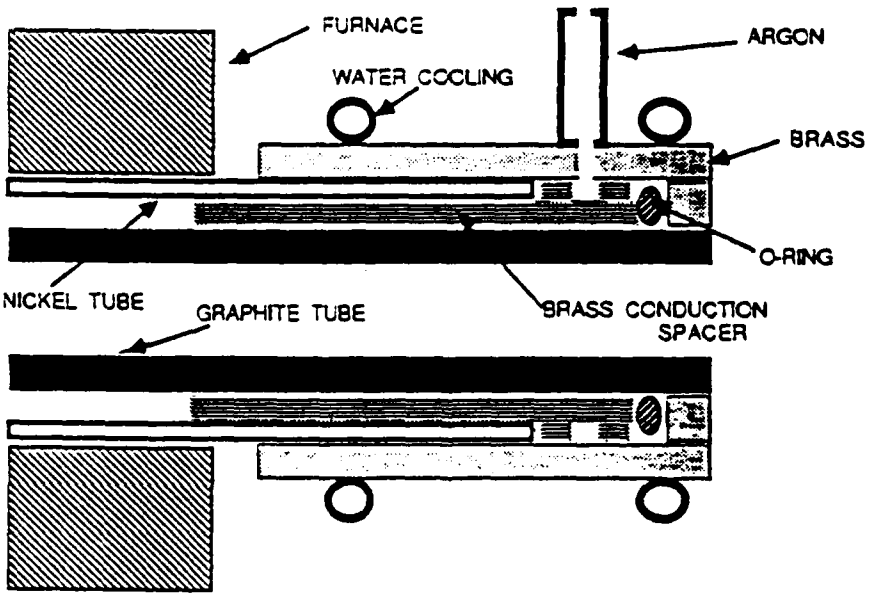

Fig. 19(b): Schematic diagram of one end of new HF synthesis furnace containing a graphite reaction tube surrounded by a Ni protection tube between which flows Ti purified argon through a special brass conduction spacer. HF and/or argon is used inside the graphite tube during synthesis or annealing experiments.

removed before they had a chance to do the graphite tube or the fluorides any harm. Great care was also taken to avoid introducing contaminants with the vitreous carbon boats which contained the fluorides. These were vacuum-baked between runs and stored and transported in a manner similar to the fluorides.

An important result of our thermodynamic analysis and experimental work to date was the recognition that during synthesis and growth, a reactive HF atmosphere is only needed during initial heat-up. Once at temperature, long reactions, annealing, or crystal growth can be done in purified argon, which is much less reactive and toxic than the HF atmosphere.

Some preliminary experiments were performed to verify some of Ravez and Dumora's [43] work. Table 2 and 3 give the x-ray diffraction results of pressed pellets of various compositions heated for 48 hours in either HF or in sealed tubes at 800°C and 500°C respectively. The x-ray pattern for the 50% composition reacted at 500°C in a sealed tube showed only a single phase. The composiiton of this phase therefore must be $PbAlF_5$ by conservation of mass considerations, validating the work of [43]. These experiments however were not run under ideal conditions, purity, etc. Also verified in these experiments was the existence of the $Pb_9Al_2F_{24}$ phase reported by the same authors.

c. Crystal Growth

Early in the program, before the detailed thermodynamic analysis was undertaken, a series of experiments were run to determine the possible problems which might be encountered during the crystal growth of the lead aluminum fluoride compounds described by Shore and Wanklyn and Ravez. A description of these growth experiments are given in Table 4. In these experiments, most compositions were synthesized by fusion of the binary fluorides in a graphite tube furnace heated by SiC elements. Anhydrous HF gas flowed over the sample which was held in a vitreous carbon boat.

The fused samples were then transferred to an ATJ grade cylindrical graphite crucible containing a conical bottom which terminated in a tapered capillary section varying from 1-2 mm diameter and 2.5 cm in length in which nucleation and growth was initiated. The crucible was ~ 1.2 cm diameter and

TABLE 2

X-ray Analysis of Samples Synthesized in HF at 800°C

Mole % PbF_2:	50	53	58	60	62	67
Phases Found:	F+AlF_3	F+AlF_3	F+PbF_2	F+PbF_2	F+PbF_2	F+PbF_2

(F = $Pb_3Al_2F_{12}$ or $PbAlF_5$)

TABLE 3

X-ray Analysis of Samples Synthesized at 500°C in a Sealed Tube

Mole % PbF_2:	40	46	50	56	60
Phases Found:	F+AlF_3	F+AlF_3	F	F+Pb_9Al_2	F+Pb_9Al_2

(F = $PbAlF_5$ or Pb_3AlF_{12}, Pb_9Al_2 = $Pb_9Al_2F_{24}$)

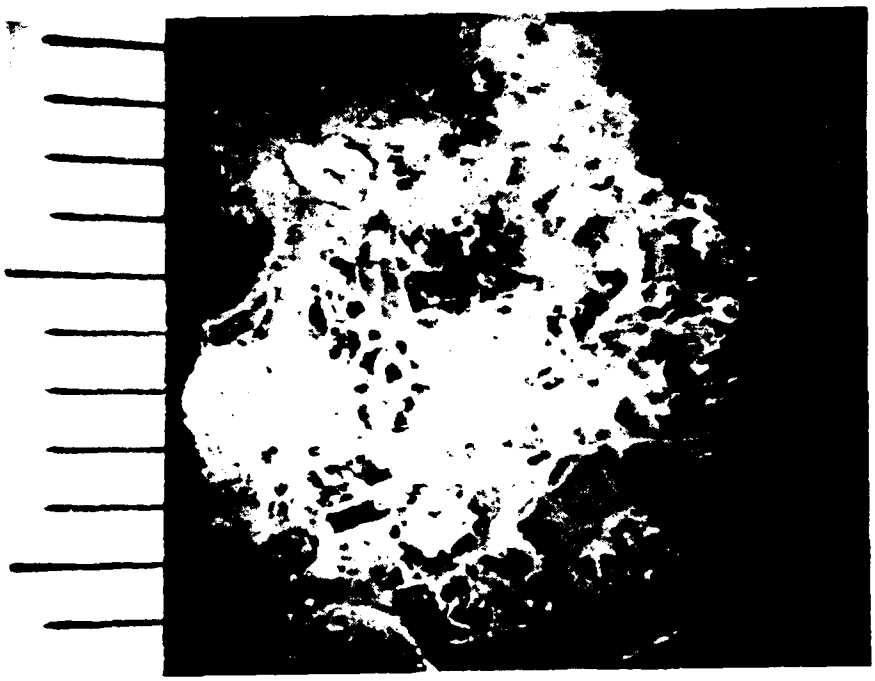

Fig. 20: Cross-sectioned slice from $Pb_3Al_2F_{12}$ boule #6 (Table 4).

TABLE 4

Early Vertical Bridgman Experiments on the Growth of Lead Aluminum Fluoride

Growth Experiment #	Melt Composition Mole % / Synthesis Method	Growth Conditions* Lowering Rate	Max. Furnace Temp.	dT/dx (°C/cm)	Results General Comments	X-ray Diffraction Analysis
1	50 / AlF_3 + PbF_2 900°C in HF	6 mm/hr	700°C	24	Excessive mass loss during synthesis. Boule transparent at bottom and top.	bottom: $Pb_3Al_2F_{12}$ + $Pb_9Al_2F_{24}$ top: AlF_3 + $Pb_3Al_2F_{12}$
2	53 / AlF_3 + PbF_2 900°C in HF	0.5 mm/hr	700°C	24	25% less material loss in synthesis. Boule transparent at bottom - opaque white at top	bottom: $Pb_3Al_2F_{12}$ top: AlF_3 + $Pb_3Al_2F_{12}$
3a	60 / AlF_3 + PbF_2 900°C in HF	1 mm/hr	700°C	24	Similar to above	bottom: $Pb_3Al_2F_{12}$ + $Pb_9Al_2F_{24}$ top: AlF_3 + $Pb_3Al_2F_{12}$
3b	60 / pregrown for 3a	1 mm/hr	700°C	24	Larger transparent region at bottom	bottom: $Pb_3Al_2F_{12}$ + $Pb_9Al_2F_{24}$ top: AlF_3 + $Pb_3Al_2F_{12}$
4	67 / AlF_3 + PbF_2 800°C in HF	0.5 mm/hr	700°C	24	No opaque white region at top. Eutectic structure in middle.	entire boule: $Pb_3Al_2F_{12}$ + $Pb_9Al_2F_{24}$
5	62 / AlF_3 + PbF_2 900°C in HF	0.5 mm/hr	700°C	24	Translucent bottom. Top 5 mm opaque transparent surface, milky center.	bottom: $Pb_3Al_2F_{12}$ middle: $Pb_3Al_2F_{12}$ + $Pb_9Al_2F_{24}$ top: AlF_3 + $Pb_3Al_2F_{12}$
6	58 / AlF_3 + PbF_2 900°C in HF	0.5 mm/hr	700°C	24	Larger opaque white region (See fig. 20)	bottom: $Pb_3Al_2F_{12}$ middle: $Pb_3Al_2F_{12}$ + $Pb_9Al_2F_{24}$ top: AlF_3 + $Pb_3Al_2F_{12}$
7	70 / AlF_3 + PbF_2 800°C in HF	0.5 mm/hr	700°C	24	Most of the boule is milky.	$Pb_3Al_2F_{12}$ + $Pb_9Al_2F_{24}$
8	73 / AlF_3 + PbF_2 900°C in HF	0.5 mm/hr	700°C	24	Most of the boule is milky with Pb droplets at rim of top.	entire boule: $Pb_3Al_2F_{12}$ + $Pb_9Al_2F_{24}$
9	58 / AlF_3 + PbF_2 850°C in HF	0.5 mm/hr	800°C	24	Boule transparent on bottom, opaque white at top.	$Pb_3Al_2F_{12}$ + $Pb_9Al_2F_{24}$ middle: $Pb_3Al_2F_{12}$ + $Pb_9Al_2F_{24}$ top: AlF_3 + $Pb_3Al_2F_{12}$
10	50 / AlF_3 + PbF_2 850°C in HF	0.75 mm/hr	800°C	39	Bottom 2/3 portion translucent, top white & frothy	
11	60 / AlF_3 + PbF_2 850°C in HF	0.75 mm/hr	800°C	39	Boule mostly translucent, small transparent section at bottom.	
12	60 / AlF_3 + PbF_2 850°C in HF	0.75 mm/hr	850°C	39	One side of boule translucent, other milky.	
13	60 / AlF_3 + PbF_2 850°C in HF	0.5 mm/hr	850°C	20	Boule mostly translucent. No large grains.	
14	60 / NH_4F + HF added to growth	0.5 mm/hr	850°C	20	Black coating on boule - poor quality.	
15	60 / "oxide free" PbF_2 (Cerac) + twice sublimed AlF_3	0.5 mm/hr	850°C	20	Boule mostly translucent but poor optical quality.	
16	60 / "oxide free" PbF_2 (Cerac) + twice sublimed AlF_3	0.5 mm/hr	850°C	37	Best result obtained. Clean at bottom but cracked larger Bridgman crucible (See fig.25)	

* Graphite Bridgman crucible grade ultracarbon (F-5, 1/2" ID tapered except No. 16 3/4" ID, purified Ar over hot Ti sponge.

4 cm long above the tapered region. The crucible was covered with a threaded lid and suspended in the furnace on a PT wire. It was lowered through the Kanthal resistance furnace in which purified argon flowed at a rate of 3 ft^3/hr. The typical axial temperature gradient at the growth interface was about 25°C/cm. Various compositions and growth rates were used. Many of the boules had large transparent or translucent regions, but cracking and polycrystallinity were often present along with other defects such as inclusions, (voids and free lead) eutectically solidified regions, and other multiphase regions as shown in fig. 20. The exact structures and quality depended upon the exact growth conditions, starting composition and purity, etc.

A significant problem we repeatedly encountered when working with lead fluoride/aluminum fluoride melts was segregation of solid AlF_3 to the top of the melt. The AlF_3 solid in AlF_3-rich melts formed a slush at the melt surface and contained numerous bubbles which persisted up to 900°C, the maximum temperature used in these experiments. This phenomena not only prevented us from obtaining homogeneous melts at compositions above approximately 35 mole percent aluminum fluoride but shifted the melt composition in the region of the growth interface toward the eutectic composition. At compositions around 40 mole percent AlF_3, large (0.5 cc) crystals of AlF_3 with negligible PbF_2 content were found at the top of the melt during vertical Bridgman growth, but these were cracked by AlF_3's ferroelastic transition at around 450°C.

The presence of inclusions together with severe cracking, which limits the size of crystals which can be cut from the boules, suggested that a major effort must be focused on purification. Fusion under HF alone did not appear to be an adequate procedure to reduce moisture-related impurites to acceptable levels. We therefore tried, in this early phase of the work, a number of alternative procedures aimed at reducing oxide and hydroxide levels in the starting materials. These included the use of decomposing teflon to liberate CF_4 and C_2F_4, and distillation in an HF atmosphere. Table 5 shows the results of inert gas fusion analysis of various samples by Oregon

TABLE 5

Summary of Inert Gas Fusion Oxygen Analysis
on Variously Treated Samples of PbF_2, AlF_3, and $Pb_3Al_2F_{12}$

Code	Sample	Source	Composition	Treatment	O_2 wt%
	AlF_3	J. M.*		as received	4.63
	PbF_2	J. M.		as received	.60
	$Pb_2Al_3F_{12}$ #12	J. M.	54:46	Reacted in HF	.31
	$Pb_2Al_3F_{12}$	J. M.	60.40	Grown Boule #11 for Table 4	.34
T-1	$Pb_2Al_3F_{12}$	J. M.	60.40	Reacted in CO_2-Teflon	1.51
T-2	$Pb_2Al_3F_{12}$	J. M.	50:50	Reacted in CO_2-Teflon	1.47
T3-1	$Pb_2Al_3F_{12}$ #21	J. M.	60:40	Synthesis in CO_2-Teflon	1.28
T3-2	$Pb_2Al_3F_{12}$ #21	J. M.	60:40	Center of boule	1.05
T3-3	PbF_2	J. M.		Melted in HF	.50
T3-4	AlF_4	J. M.		Sublimed in vacuum	.98
S-1	PbF_2	J. M.	From the same run	Sublimed in HF (sublimate)	1.19
S-2	PbF_2	J. M.		Residue	1.03
S-3	PbF_2	J. M.		Initial Starting Material	1.06
S-4	AlF_4	J. M.		as received	2.66
Z-1	AlF_4	J. M.		Sublimed 2x in vacuum	.705
Z-2	PbF_2	Cerac		as received	.850
Z-3	AlF_3	J. M.		sublimed 1x in vacuum	.671
Z-4	AlF_3	J. M.		as received	2.25
Z-5	$Pb_2Al_3F_{12}$ #22	J. M.		Reacted from sublimed AlF_3 + HF melted PbF_2	1.04
Z-6	$Pb_2Al_3F_{12}$ #23	J. M.& Cerac		Reacted from 2x sublimed AlF_3 + Cerac PbF_2	1.00

Metallurgical Corporation. From this table one can see that the lowest oxygen content was obtained by subliming the AlF_3 (samples Z-1 and Z-3) and reacting the starting materials together under HF. The oxygen level in the AlF_3 (sample Z-1, Table 5) was measured as 0.7 wt%, and in the PbF_2 0.85%. Since Johnson Matthey "Puratronic" grade AlF_3 was found to contain 2.25% of oxygen, the improvement produced by distillation was significant, but the occurrence of around 1% oxygen in these crystals was still too high for good quality crystal growth.

Table 6 shows that if the powdered samples were sufficiently exposed to humidity prior to analysis that one could not determine the effect of careful purification and storage procedures. Although we do not know the actual starting O_2 content in the samples labeled dry, we do know that on exposure to moist air they gain weight.

The reproducibility of this method for oxygen content was not particularly good as seen from the results for PbF_2 samples 4 & 5 (Table 6) which were duplicate samples from the same source. Handling procedures just prior to analysis may be responsible here also.

From the results in Table 4, it can be seen that the best crystals were obtained using the steepest gradient, the larger Bridgman crucible, twice-sublimed AlF_3 and 60 to 63 mole percent PbF_2. The purification method which worked best for these runs was to sublime the AlF_3 (thus separating it from alumina and aluminum hydroxide), then reacting the AlF_3 together with "low moisture content" PbF_2 under a flowing HF atmosphere. Reactions done with decomposing teflon and $NH_4F \cdot HF$ did not appear as effective as the above procedure for PbF_2 + AlF_3 melts, although an extensive evaluation was not made.

We were able to obtain a large, reasonably transparent crystal of lead aluminum fluoride from a section of boule No. 16 grown from a melt with a $Pb_3Al_2F_{12}$ composition. The vertical and horizontal cross-sections of the boule given in fig. 21 show large grains, cracks and compositional and structural charges along the boule axis. The slice is 4 mm thick. As mentioned before, the starting materials for the boule were reacted under an HF envi-

TABLE 6

Effect of Intentional Exposure to Atmospheric Moisture
on the Inert Gas Fusion Oxygen and Hydrogen Analysis of PbF and AlF_3

Sample #	Material	H_2(wt%)	O_2(wt%)
1	Dry AlF_3*	0.1876	0.847
2	Wet AlF_3**	0.1690	0.910
3	Dry PbF_2*	0.0002	0.138
4	Dry PbF_2*	0.0002	0.081
5	Wet PbF_2**	0.0006	0.064
6	PbF_2+Al_2O_3 (O_2 wt% = 0.460)	0.0003	0.522

* Purified & stored in dry box prior to sending for analysis
** Intentionally exposed to atmospheric moisture before sending for analysis

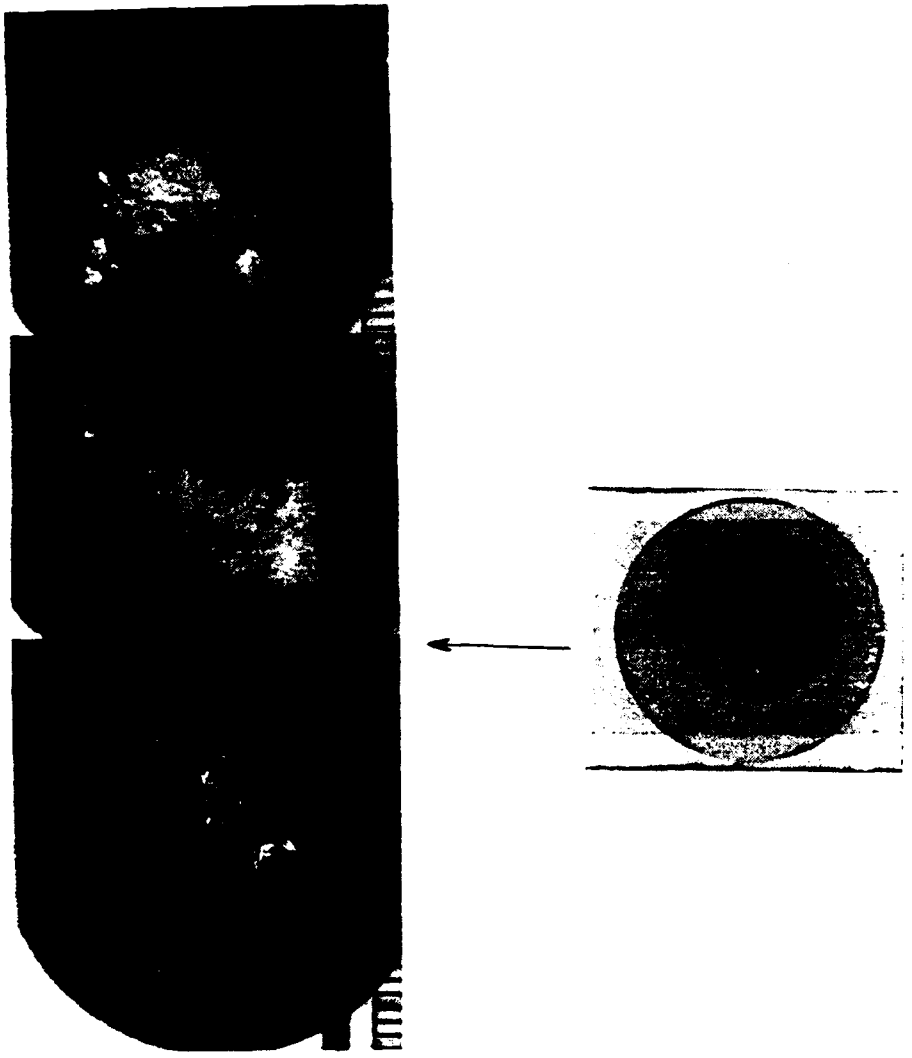

Fig. 21: Sections of a vertical cross-section of boule #16 (Table 4) showing grains, cracks, and other structural features (mm scale). Slice to right came from boule at position indicated.

ronment, then grown by the vertical Bridgman technique in a graphite crucible under flowing argon. Closer examination of the apparently clear sections showed some complex multiphase morphology as can be seen in fig. 22. This structure, which becomes more pronounced under cross-polarized light, was thought initially to be a ferroelectric domain structure, but it did not dissappear at temperatures above the reported transition temperature. It seems unlikely, therefore, that it is a domain structure unless the Curie temperature for this sample is above that reported. Dielectric measurements as a function of temperature are planned to resolve this question. It is possible that the structure results from the presence of multiple phases which may be closely related in composition. Oxygen contamination may play a role also. Samples heated above 300°C turned brown.

Other features in this and other boules indicated phase relations during growth that cannot be explained by a pseudo-binary system in equilibrium. Some of the smaller grains growing in from the crucible sides had Pb streamers running through them (see fig. 23) and there were large grains of AlF_3 at the top of the boule as can be seen in fig. 24 which shows a polished section of the boule top at a slant and obliquely lit. There were also some unusual lead fluoride-rich eutectic inclusions in the middle of the boule, suggesting interface breakdown or the lack of a well defined interface created by having a slush (solid - liquid phase) rather than a homogeneous melt. The presence of the aluminum fluoride grains would be expected from the Shore and Wanklyn phase diagram (fig 17) at compositions containing less than about 68% PbF_2. It should be the first phase to crystallize during solidification of the melt and should form at the bottom of the growth ampoule. Its occurrence at the top surface of the boule was therefore surprising. One possibility is that the AlF_3 floats to the surface after it nucleates due to the large density difference between AlF_3 (2.88 gm/cc) and PbF_2 (8.24 gm/cc). The formation of AlF_3 should, however, be avoided by using a melt composition richer in PbF_2 so that crystallization of $Pb_3Al_2F_{12}$ would occur directly from the melt as shown in fig. 17. However, some preliminary experiments did not give the desired results thus showing the importance of resolving the details of the phase diagram.

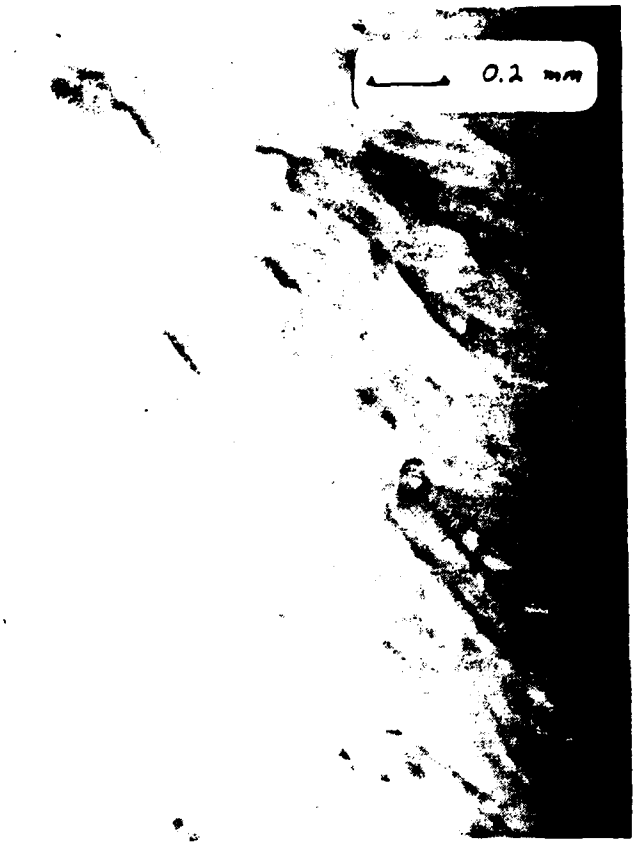

Fig. 22: Optical microscope photograph of unidentified structural features in otherwise clear section of $Pb_3Al_2F_{12}$ crystal.

Fig. 23: Pb inclusions growing from carbon crucible wall.

Fig. 24: Segregation of AlF_3 at top of a typical boule of $Pb_3Al_2F_{12}$.

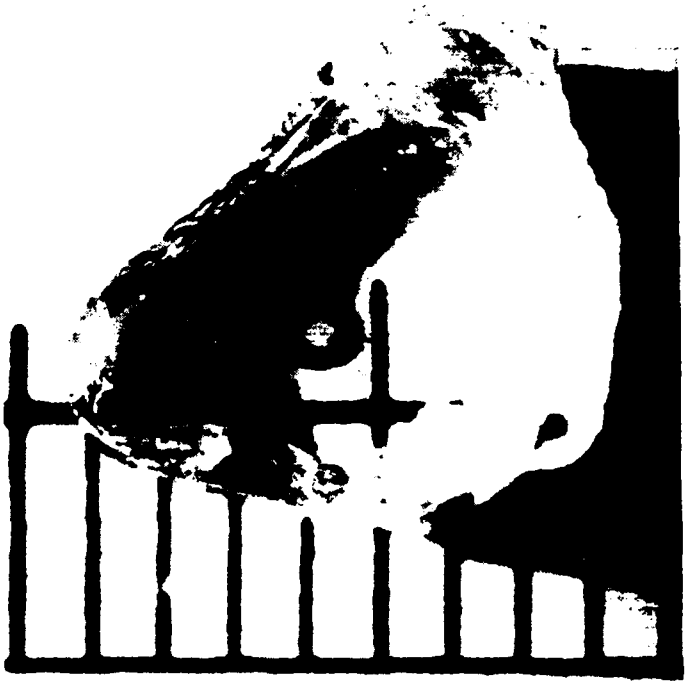

Fig. 25: Transparent piece of boule #16 upon which property measurements were made.

As mentioned previously, we hope to prevent the formation of free lead by using better starting material purification methods combined with improved materials handling techniques and improved atmosphere control during the reaction and growth steps. Since we started working on the PbF_2-AlF_3 system, we made major improvements including the Vacuum Atmospheres glove box, improved the HF synthesis furnace, modification of our DTA set-up to run with graphite sample holders with tight fitting lids, and will soon start construction of an improved growth furnace. A sealed system may be required both for long-term annealing experiments planned for part of the phase equilibria studies and during growth with lead containing fluoride melts to prevent incongruent vaporization. It was necessary to understand the cause of lead formation before sealing our samples, i.e., Pt or Au, because platinum or gold in contact with lead form alloys which melt below our operating temperatures.

Using the new improved HF furnace, 48 hour sintering annealing experiments were carried out with 50:50 and 60:40 atomic precent lead fluoride/ aluminum fluoride mixtures. These were done in an HF environment during the heating portion of the cycle to counteract contaminants that might have been resident on the furnace walls, inadvertently introduced during handling, or present in the source materials, which were not purified. Two annealing temperatures were used, 550 and 620°C. The samples were then analyzed by studying their x-ray diffraction patterns. The samples annealed at 550° did not appear to reach equilibrium in 48 hours, while those annealed at 620° did (for these two compositions). In all cases there was weight loss of 1-2%. These preliminary results seem to confirm that at least under these conditions the stoichiometry of the intermediate lead aluminum fluoride compound has the 60:40 composition instead of or possibly in addition to the 50:50 phase found by Ravez et al. Since the 60:40 structure belongs to a family which is also generally ferroelectric, and may be what Ravez et al. measured, this does not represent a serious problem. More extensive experiments under a variety of conditions will be carried out to elucidate what is actually going on in this system.

d. Property Measurements

A transparent section from boule No. 16 as shown in fig. 25 was investigated by a number of techniques including optical microscopy, x-ray Laue analysis, and optical absorption spectroscopy. A few small voids can be seen in the photograph in fig. 25 and the "domain-like" structure described earlier can be observed easily in this sample in cross-polarized light. The isogyre pattern revealed under polarized light normal to the polished surface is shown in fig. 26 and indicates that this crystal grew with its c-axis very near to the boule axis (normal to the polished face). The well-formed isogyre pattern suggests that the crystal is of reasonably good optical quality without much strain, in spite of the "domain-like" structure present. The crystal quality and the c-axis orientation can also be observed in the back-reflection x-ray Laue photograph shown in fig. 27 where the four fold symmetry is clearly evident.

Density measurements were made on the above specimen using Avogadro's principle, i.e. finding the sample volume by its fluid displacement. Kerosine was used in these experiments. A value of 6.64 gm/cc was measured which compares well with Shore and Wanklyn's [27] experimental value of 6.47 for the $Pb_3Al_2F_{12}$ phase. Our value may be off somewhat due to the rough sample surfaces but is much closer to [27] then to the $PbAlF_5$ phase of Ravez and Dumora [43] who's values of 5.956 (calculated) and 5.91 (experimental) are very low by comparison. This is an important piece of information tending to confirm the existence of $Pb_3Al_2F_{12}$ phase and the composition of our sample.

Optical absorption measurements were made in the UV-visible region with a Perkin-Elmer spectrophotometer and the IR measurements with an IBM FTIR. The combined data is given in the transmission vs. wavelength plot of fig. 28. The long wavelength edge begins at about 8 μm and zero transmittance occurs at about 9 μm. The short wavelength edge was found to be at 0.29 μm. This broad transparency range is typical of fluoride crystals. PbF_2, for example, is transparent from 0.29 to 11.6 μm. Several small absorption peaks were observed near 2.7 and 6 μm and are probably due to bound H_2O and also adsorbed H_2O on the crystal surface.

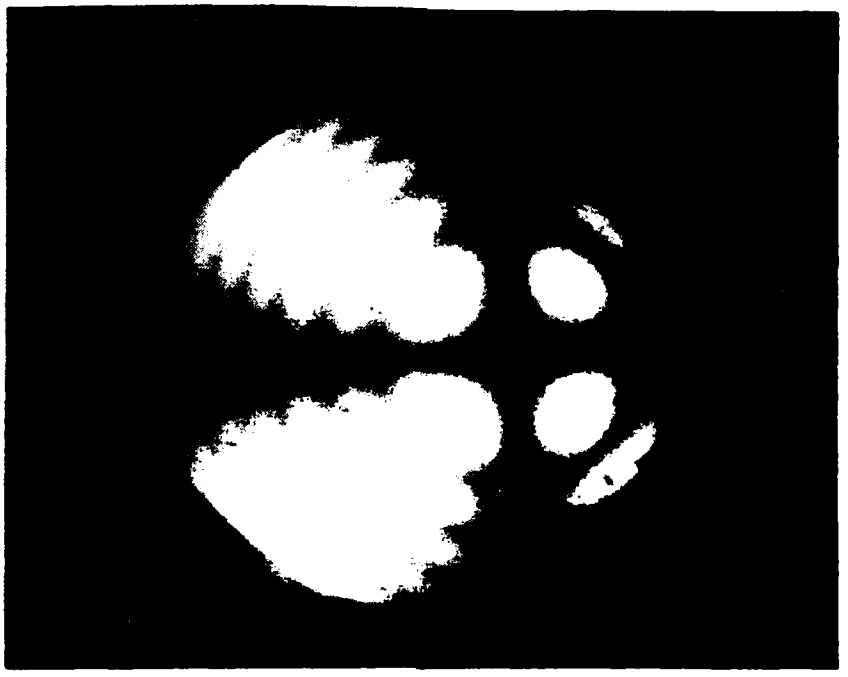

Fig. 26: Conoscopic figure taken in the direction perpendicular to the face shown in fig. 25. Viewing direction is down the growth axis.

Fig. 27: Back-reflection Laue photograph of sample in fig. 25 showing four-fold symmetry in growth direction.

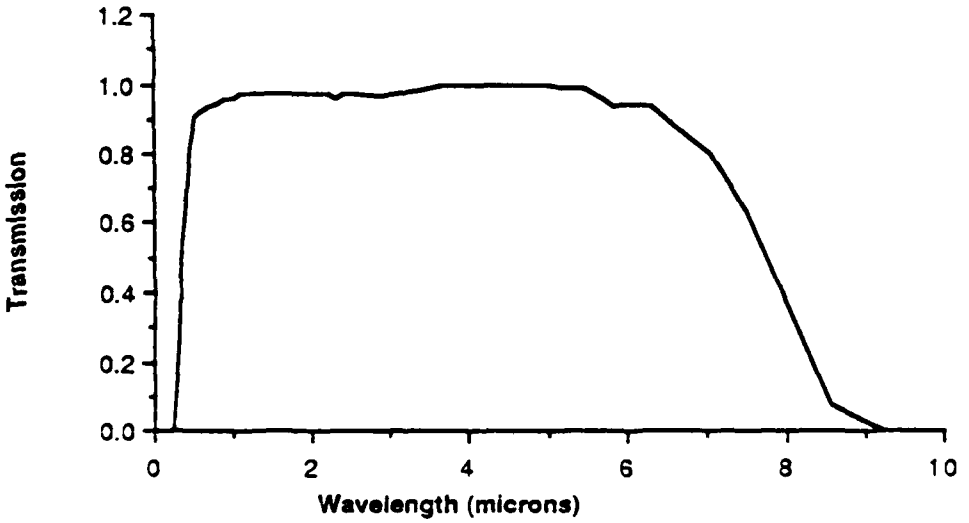

Fig. 28: Relative spectral transmittance of lead aluminum fluoride crystal. Some small absorption peaks, probably associated with bound and adsorbed H_2O, can also be seen.

Dielectric constant measurements on this crystal gave a value of around 1800, and changed only slowly with temperature.

IV. FUTURE PLANS

Under a separate contract we should, during the next year, conclusively identify the compounds which form in the PbF_2-AlF_3 system and their thermodynamic properties, and also have significant results in the PbF_2-GaF_3 phase diagram. A technique is now being employed using purified materials in covered graphite DTA crucibles and occasionally hermetically sealed platinum capsules. Long-term annealing and differential thermal analysis work can be carried out without significant component loss or contamination from the environment by this method. Dr. Newkirk at the Lawrence Livermore Laboratories has been helping us with some supplies and equipment in this phase of the project.

We also have designed and will soon construct an improved Bridgman crystal growth system using the insight and knowledge we have gained from our thermodynamic systems analysis and our knowledge of the phase fields present in this system. Our understanding of the thermodynamic stability of the compounds of interest as well as their interaction with the environment around them should lead to significantly improved results and large high quality single crystals. The crystals produced will be characterized in detail with particular emphasis on their composition, structure, homogeneity, and their ferroelectric properties.

V. CONCLUSIONS

During the course of this investigation, crystals of $ScTaO_4$, $ScNbO_4$, $SrAlF_5$, $Pb_3Al_2F_{12}$ ($PbAlF_5$), $BaTiO_3$, and $Sr_xBa_{1-x}TiO_3$ solid solutions were grown. The $ScTaO_4$ crystals grown in this program were of a previously undiscovered high temperature tetragonal phase and high quality $BaTiO_3$ produced. Large crystals of $SrAlF_5$ were grown by the Bridgman method, but the material lacks a high dielectric constant at mm wave frequencies and studies on this material were not pursued. A more promising material, a compound in the PbF_2-AlF_3 system, became the focus of our attention during the later part of this program. A large crystal of a compound now believed to be $Pb_3Al_2F_{12}$ was

grown and some of its properties measured. This and other crystals of this material contained optical inhomogeneities however, and the resulting microstructure may have resulted from the presence of more than one PbF_2-AlF_3 phase or oxygen contamination. Thermodynamic studies and crystal growth of compositions in the PbF_2-AlF_3 and PbF_2-GaF_3 systems are proceeding (under a new ONR contract) using improved techniques to minimize contamination, and considerable insight into the requirements for the growth of high quality lead aluminum fluoride crystals has been gained.

VI. REFERENCES

1. M. B. Klein, Int. J. of Infrared and Millimeter Waves, 2, 239 (1981).
2. G. D. Boyd, T. J. Bridges, M. A. Pollack, and E. H. Turner, Phys. Rev. Lett., 26, 387 (1971).
3. G. D. Boyd and M. A. Pollack, Phys. Rev., B7, 5354 (1973).
4. W. L. Zhong, P. L. Zhang, and H. C. Chen, Solid State Communications, 49 (1984) 467.
5. J. Ravez, S. C. Abrahams, J. P. Chaminade, A. Simon, J. Grannec, and P. Hagenmuller, Ferroelectrics, 38, 773 (1981).
6. S. C. Abrahams, J. Ravez, A. Simon, and J. P. Chaminade, J. Appl. Phys., 52, 4740 (1981).
7. J. M. Palau and L. Lassabaterre, C. R. Acad. Sci. Paris, 273, 714 (1971).
8. Landolt-Bornstein "Numerical Data and Functional Relationships in Science and Technology," New Series 16 (Ferroelectrics and Related Substances), Springer-Verlag (1981).
9. J. A. Basmajian and R. C. De Vries, J. Am. Ceram. Soc., 40 [11], 374 (1957).
10. R. M. Henson and A. J. Pointon, J. Crystal Growth, 26, 174 (1974).
11. H. J. Scheel, J. Crystal Growth, 13/14, 560 (1972).
12. W.-S. Liu, M. F. Wolf, and D. F. Elwell, "Vibrational Stirring: A New Method for Rapidly Mixing Solutions and Melts During Growth," J. Crystal Growth, 82, 589 (1987).

37. R. C. Pastor and K. Arita, Mat. Res. Bull., 11, 1037 (1976).

38. R. C. Pastor and M. Robinson, Mat. Res. Bull., 11, 1327 (1976).

39. R. C. Pastor, M. Robinson, and M. Braunstain, Mat. Res. Bull., 15, 469 (1980).

40. B. M. Wanklyn, J. Crystal Growth, 5, 279 (1969).

41. J. P. Meehan and E. J. Wilson, J. Crystal Growth, 15, 141 (1972).

42. P. Selgert, N. R. Whippey and W. Assmus, J. Crystal Growth, 69, 198 (1984).

43. J. Ravez and P. Dumora, C. R. Acad. Sci., 269, 331 (1969).

44. J. Ravez, R. von der Muhll, and P. Hagenmuller, J. Solid State Chem, 14, 20 (1975).

45. K. L. Kmvob, J. W. Hartie, and J. L. Margrave, Trans. Faraday Soc., 64, 361 (1968).

Appendix

ONR Contract #N00014-82-K-0266

Index of all technical reports:

Annual Technical Report, May 1983, CMR-83-8
Semi-Annual Technical Report, November 1983, CMR-83-11
End-of-the-Fiscal-Year Report, October 1985, CMR-85-5

Publications:

Crystal Growth of a New Tetragonal Phase of $ScTaO_4$ by D. Elwell, W. L. Kway, and R. S. Feigelson, J. Crystal Growth, 71, 237 (1985).

END

9-87

DTIC